

Topology of rotating stratified fluids with and without background shear flow

Ziyan Zhu,¹ Christopher Li,² and J. B. Marston³

¹*Stanford Institute for Materials and Energy Sciences,*

*SLAC National Accelerator Laboratory, Menlo Park, CA 94025, USA**

²*Department of Physics, Brown University, Providence, RI 02912-1843, USA*

³*Brown Theoretical Physics Center and Department of Physics,
Brown University, Providence, RI 02912-1843, USA*

Poincaré inertio-gravity modes described by the shallow water equations in a rotating frame have non-trivial topology, providing a new perspective on the origin of equatorially trapped Kelvin and Yanai waves. We investigate the topology of rotating shallow water equations and continuously stratified primitive equations with and without background shear flow. Continuously stratified fluids support waves analogous to the edge modes of weak three-dimensional topological insulators. Background shear flow not only breaks the Hermiticity and homogeneity of the system but also leads to instabilities. By introducing a gauge-invariant winding number, we show that singularities in the phase of the Poincaré waves of the unforced shallow-water equations and primitive equations persist in the presence of both horizontal and vertical shear flows. Thus the bulk Poincaré bands have non-trivial topology and we expect and confirm the persistence of the equatorial waves in the presence of shear along the equator where the Coriolis parameter f changes sign.

I. INTRODUCTION

Oceanic and atmospheric waves share fundamental physics with topological insulators and the quantum Hall effect, and topology plays an unexpected role in the movement of the atmosphere and oceans [1]. Topology guarantees the existence of unidirectional propagating equatorial waves on planets with atmospheres or oceans. In particular, there is a topological origin for two well-known equatorially trapped waves, the Kelvin and Yanai modes, caused by the breaking of time-reversal symmetry by planetary rotation. Coastal Kelvin waves have also been demonstrated to have a topological origin [2]; thus Kelvin’s 1879 discovery of such waves [3] likely marked the first time that edge modes of topological origin were uncovered in any context (though the topological nature remained hidden). Recently reanalysis observations of Poincaré-gravity waves in the stratosphere have been used to demonstrate the non-trivial topology of these waves [4]. In light of these discoveries, it is important to consider the generalization of the shallow water equations to the more general problem of continuously stratified fluids. At the same time, it is also crucial to consider fluids driven by shear flows and damped by friction. Such extensions bring greater realism to models of actual fluids both on Earth [5] and on other planets [6]. The extension to background shear may also pave the way to the treatment of nonlinearities through the use of the mean-field quasilinear approximation [7–9] that self-consistently treats the interaction of waves with mean flows.

The existence of topological edge modes can be understood, via the principle of bulk-interface correspondence, to be predicted by the non-trivial topology of bulk modes. Bulk-interface correspondence has been invoked for the quantum Hall effect and topological insulators [10, 11] as well as for a variety of classical wave systems, including nanophotonics [12–15], acoustics [16–18], mechanical systems [19, 20], continuum fluids [1, 2, 21–23] and plasmas [24–26]. The principle is clearest for Hermitian systems. Driving and dissipation however lead to non-Hermitian dynamics [27–31]. By continuity, weak damping and driving may be expected to only change the waves slightly, but what happens as the forcing increases? Efforts have been put into the topological classification of non-Hermitian systems [32–35]. Whether or not bulk-interface correspondence continues to hold remains a central problem. It has been argued that traditional bulk-interface correspondence breaks down in non-Hermitian systems [36, 37]. Alternatives to the topological Chern number have been proposed [33, 38–41]. Non-Hermitian bulk-interface correspondence has also been explored experimentally [42, 43]. Here, we show that the phase singularity in the bulk wavefunctions persists in the presence of shear flow. The phase of the bulk Poincaré modes exhibits a vortex or anti-vortex at the origin in the wavevector space, with a change in the phase winding number across the equator. We show that equatorial Yanai and Kelvin waves persist in the background shear, consistent with the continued applicability of the principle of bulk-interface correspondence in the non-Hermitian realm.

The paper is organized as follows. A brief introduction to topology in the context of fluid systems is presented in Section II. It includes references to some pedagogical reviews. We derive the shallow water equations in the

* ziyanzhu@stanford.edu

presence of shear and compare numerical and perturbative methods to find the wave spectrum in Section III. The continuously stratified primitive equations with and without shear are analyzed in the f-plane approximation in Section IV and the Chern number for each band is found following the procedure introduced in Ref. [1], demonstrating a correspondence with weak 3D topological insulators. In Section V, we show that the system is unstable with both horizontal and vertical shear. In Section VI we numerically calculate the winding number to demonstrate the topology of the bulk. We first show that bulk-interface correspondence holds in the case of spatially varying Coriolis parameters. (The reader may wish to look at Ref. [4] which attempts to make the topological concepts discussed here accessible to climate scientists and geophysical fluid dynamicists.) We then show our main result, which is that bulk-interface correspondence also appears to hold as background shear is turned on and the dynamics become non-Hermitian. Discussion and concluding remarks are made in Section VII. Some details of the calculations are relegated to Appendices.

II. TOPOLOGICAL INVARIANTS AND BULK-INTERFACE CORRESPONDENCE

Topology is the branch of mathematics concerned with the qualitative shapes of objects that remain unchanged under continuous deformations. The topological equivalence of a donut and a coffee mug (both have a single hole) is a commonly mentioned example, as is the fact that an Möbius strip cannot be made orientable without tearing the paper and that it is impossible to comb the spines of a hedgehog (the Hairy Ball Theorem).

Topology finds noteworthy applications in fluids. Vortex rings for instance show persistence that is rooted in topology. The persistence of vortex rings was striking enough for William Thomson (Lord Kelvin) to attempt to develop a theory of atoms based upon vortex rings in the hypothetical aether. Kelvin’s circulation theorem states that the circulation (the line integral of the fluid velocity) around a closed loop that is advected with the fluid and thus deformed by the internal motion remains constant in the absence of viscosity and forcing. Tornadoes, hurricanes, Jupiter’s red spot, and even cutoff low-pressure regions in Earth’s atmosphere and vortex loops in the ocean are all examples of persistent vortices.

Topology may also be applied to more abstract mathematical spaces. In work recognized by the 2016 Nobel Prize in Physics, David Thouless and his collaborators demonstrated that the quantized conductance of the integer quantum Hall effect can be understood mathematically in terms of the topology of complex-valued wavefunctions that live on a compact Brillouin zone [44]. The electrical Hall conductance is proportional to an integer Chern number that characterizes the topology of the wave functions. This quantization has a physical interpretation as electrical currents that propagate around the boundary of the semiconducting material in discrete modes, modes that owe their existence to the principle of bulk-interface correspondence. The principle states that non-trivial topology away from a boundary implies the existence of unidirectional waves trapped along the boundary. The quantum of resistance, h/e^2 , can be measured so precisely that it has now been adopted as the international standard of resistance.

The topology of linearized wave equations is frequently quantified in terms of the Chern number [45]. See Refs. 4, 46–48 for some pedagogical reviews. However, the Chern number has a number of drawbacks. In contrast to systems on spatial lattices (where the Chern number was first applied), for continuous systems such as fluids the Chern number need not be integer-valued as it depends on how an integral over the Berry curvature is regularized at high wavevectors. This ambiguity can sometimes be avoided by compactification [1, 2]. Our viewpoint here is that this is more of a mathematical problem than a physical one because at small scales dissipation becomes strong providing a natural (albeit non-Hermitian) regularization at high wavenumbers. Ultimately at the smallest scales, the fluid description passes over to Hamiltonian molecular dynamics. It is unclear how to extend the Chern number to systems with dissipation, driving, or nonlinearities – all properties of real fluids.

By contrast, these ambiguities do not arise for a winding number invariant. To demonstrate the concept of the winding number, it is necessary to define the gauge-invariant, complex-valued quantity Ξ in the frequency-wavevector space:

$$\Xi(k_x, k_y) \equiv h^*(k_x, k_y) v(k_x, k_y), \quad (1)$$

where h is the height and v is the meridional velocity. Normal wave modes, which are defined only up to an overall phase and magnitude, have their overall phases cancel out in Eq. (1), leaving only the relative phase difference between h and v and making Ξ gauge-invariant.

The idealized rotating shallow-water model on the f-plane is an illustration of the winding number. Figure 1 shows the positive and negative frequency Poincaré modes (inertio-gravity waves) and the zero-frequency geostrophically balanced mode. The geostrophically balanced mode becomes Rossby waves if the Coriolis parameter varies with latitude. The topology of Poincaré-gravity modes is characterized by a vortex or antivortex in the frequency-wavevector space, with winding number ± 1 . A winding number of $+1$ means Ξ increases (decreases) by 2π as one moves around

the center of the vortex in a clockwise (counterclockwise) sense. On the other hand, the winding number of the geostrophic balanced mode is 0 (topologically trivial). The winding number, as an alternative to the Chern number, serves the same function by quantifying the topology of the bands.

A band inversion is a phenomenon where the winding number flips sign. This can occur for the Poincaré-gravity waves when either the Coriolis parameter or the wave frequency changes sign. According to the bulk-interface correspondence, the number of waves that traverse the otherwise forbidden region in the frequency space is the change in the winding number, which is 2 in this case.

Spectral flow in frequency-wavevector space as the zonal wavenumber increases shows that the negative frequency Poincaré band loses two modes, the geostrophic band gains and loses one mode and the positive frequency Poincaré band gains the two modes. These are the equatorial Kelvin and Yanai waves (The Yanai waves are also called mixed Rossby-gravity waves). The two equatorial modes move with an eastward group velocity at all zonal wavenumbers, and this unidirectional propagation is a consequence of the breaking of time-reversal invariance by the planetary rotation.

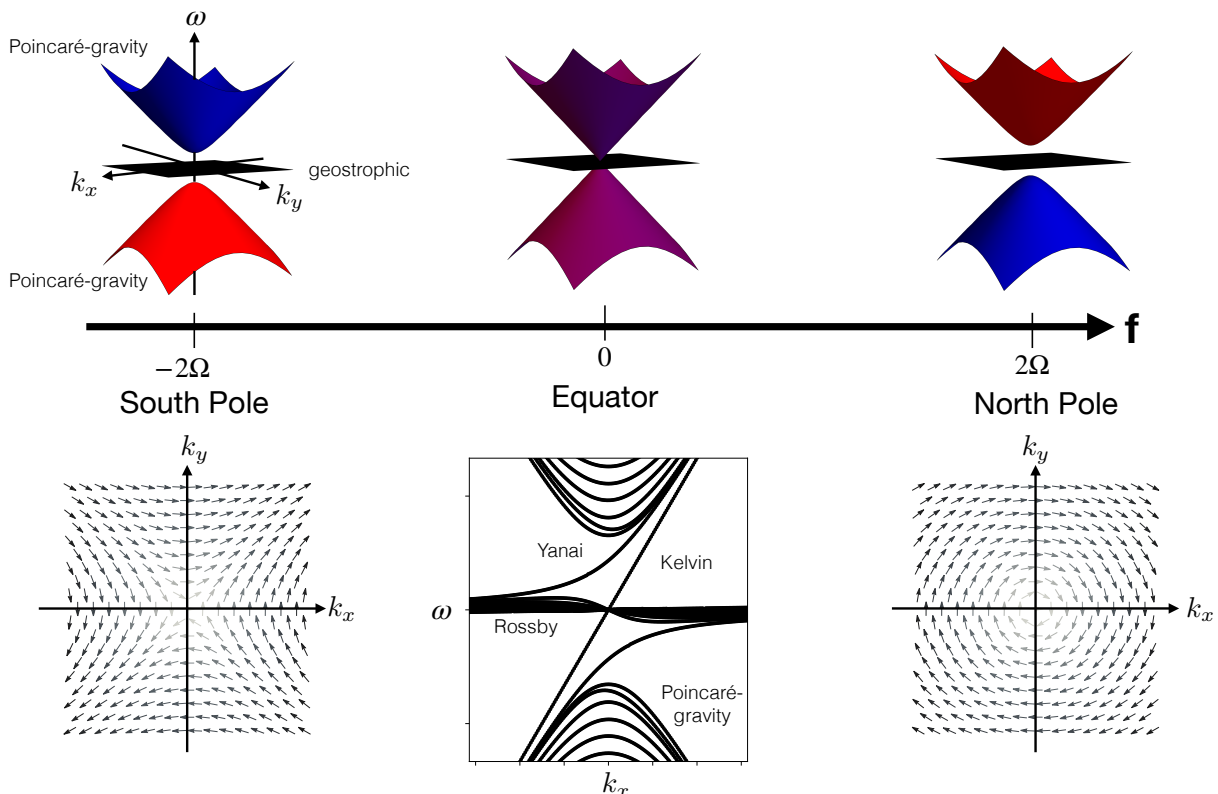


FIG. 1: Dispersion relation in frequency-wavevector space of the rotating shallow water equations in the f -plane approximation as a function of latitude. The upper and lower bands are positive and negative frequency modes of the Poincaré waves, and the color indicates the sign of the winding number of the upper band (blue = -1 , red = $+1$) as shown by the plots of the argument of $\Xi(k_x, k_y)$ in the lower half of the figure (see text). At the equator $f = 0$, the frequency gap vanishes in a Weyl point, and a topological transition occurs (purple) as the two bands invert. The subinertial range has only a zero frequency band (black) containing modes in exact geostrophic balance. The inset shows the dispersion relation on the equatorial β -plane with the quasi-geostrophic Rossby waves, the Poincaré waves, and the unidirectional Kelvin and Yanai waves. The vectors plot corresponds to the south pole (left) and the north pole (right) respectively. (Figure and caption adapted from Ref. [4].)

III. ROTATING SHALLOW WATER EQUATIONS WITH HORIZONTAL SHEAR

We begin this section by presenting the linearized rotating shallow water equations in the presence of horizontal shear and later consider vertical shear in the continuously stratified primitive equations. (See Chapter 5 on “Zonally symmetry wave – mean interaction theory” of Ref. [49] for relevant background.) Note that x and y are zonal and meridional coordinates respectively. For simplicity we only consider shearing flow moving in the x -direction

$\mathbf{U}(y) = (U(y), 0)$. We first introduce the following dimensionless quantities:

$$\tilde{t} = 2\Omega t, \quad \tilde{\eta} = \frac{\eta}{H}, \quad \tilde{H}(y) = 1 + \frac{h(y)}{H}, \quad \tilde{\mathbf{u}} = \frac{\mathbf{u}}{c}, \quad \mathbf{U} = \frac{U}{c}, \quad \tilde{f}(y) = \frac{f(y)}{2\Omega}, \quad \tilde{\mathbf{x}} = \frac{\mathbf{x}}{L_d}, \quad (2)$$

where $c = \sqrt{gH}$ is the gravity waves speed in nonrotating shallow water equations, Ω is the planet rotation rate, H is zonally averaged depth in the absence of shear, and $L_d = c/2\Omega$ is the global Rossby radius of deformation. Note that we assume L_d is much smaller than the domain width, which allows us to treat the two equators independently. In terms of these nondimensionalized quantities and dropping the tildes for clarity, the shallow water equations after linearization and non-dimensionalization are given as follows (see Appendix A for the derivation):

$$\begin{aligned} \partial_t u + U(y)\partial_x u + v\partial_y U(y) + \partial_x \eta - f(y)v &= 0, \\ \partial_t v + U(y)\partial_x v + \partial_y \eta + f(y)u &= 0, \\ \partial_t \eta + H(y)(\partial_x u + \partial_y v) + v\partial_y H(y) + U(y)\partial_x \eta &= 0, \end{aligned} \quad (3)$$

where u, v are respectively the x and y components of fluid velocity in the horizontal directions, $f(y)$ is the Coriolis parameter, $H(y)$ is the mean layer depth and η is the fluctuation in the depth about this mean; thus the total layer depth is given by $h = H(y) + \eta$. Note that H here is a function of y due to the balance with the horizontal shear flow (see Eq. (5)) below).

We now further specialize to the case of a background basic shear flow that oscillates sinusoidally in the y -direction:

$$U(y) = U_0 \sin\left(\frac{2\pi y}{\Lambda}\right), \quad (4)$$

where U_0 is the magnitude of the shear flow measured in units of $c \equiv \sqrt{gh}$ and Λ is the wavelength of the shear. Note that linear shear $U(y) \propto y$ is incompatible with the periodic boundary conditions that we adopt in the following to eliminate any boundaries from the bulk problem that would confuse the application of the bulk-interface correspondence principle, as the only boundaries that we consider here are those located where the Coriolis parameter vanishes. Geostrophically balancing the basic flow then determines the mean depth $H(y)$, which satisfies:

$$\frac{\partial H(y)}{\partial y} = -f(y)U(y). \quad (5)$$

In the f-plane approximation $f(y) = f_0$ for a constant f_0 and the mean depth is:

$$H(y) = 1 + \frac{U_0 f_0 \Lambda}{2\pi} \cos\left(\frac{2\pi y}{\Lambda}\right). \quad (6)$$

A. Waves on a planet with two equators

To investigate whether or not bulk-interface correspondence continues to hold in the presence of horizontal shear, we first examine the dispersion relation of shallow water waves in the presence of both rotation and shear. The wave frequencies are found numerically with the open-source pseudo-spectral `Dedalus` package [50]. We employ $N_y = 61$ spectral modes in the y -direction, sufficient to resolve the waves and odd in number so that symmetry about $y = 0$ can be preserved. We check that increasing the resolution N_y does not change the frequencies significantly, including the Rossby wave frequency and the dispersion of the geostrophic modes. We choose

$$f(y) = \sin\left(\frac{2\pi y}{L_y}\right) \quad (7)$$

and set $L_y = 4\pi$ where L_y is the width of the periodic domain (Fig. 2). This choice respects the periodic boundary conditions and is sometimes called ‘‘a planet with two equators’’ as the Coriolis parameter changes sign twice across the domain [1].

Assuming the sinusoidal horizontal shear Eq. (4), which is antisymmetric about the equator located at $y = 0$, has

the same periodicity as the domain size ($\Lambda = L_y$) the mean depth is:

$$H(y) = 1 + U_0 \left[\frac{L_y}{8\pi} \sin\left(\frac{4\pi y}{L_y}\right) - \frac{y}{2} \right]. \quad (8)$$

Similarly, if the shear is symmetric about the equator at $y = 0$, namely

$$U(y) = U_0 \cos\left(\frac{2\pi y}{\Lambda}\right), \quad (9)$$

from geostrophic balance, the mean depth is:

$$H(y) = 1 + \frac{U_0 L_y}{8\pi} \cos\left(\frac{4\pi y}{L_y}\right). \quad (10)$$

We consider both profiles in the following.

In the absence of shear, Fig. 2(a), equatorial Kelvin waves and Yanai waves appear in the gap between the high-frequency Poincaré and low-frequency planetary waves. These waves have a topological origin [1]. They propagate unidirectionally (their group velocity does not change sign for all k_x), as guaranteed by topology. Note that while the wave crest of the Rossby wave indeed always has a westward component, its group velocity can be both directions, as can be seen from the wave dispersion in Fig. 2(a). As there are two oppositely-oriented equators, there are both eastward and westward propagating modes localized respectively at each equator. When shear $U_0 \neq 0$ is turned on, the planetary Rossby waves are Doppler shifted and we observe continuous spectra near the zero-frequency [51]. The continuous spectrum spans $\omega = \pm U_0 k_x$. The dispersion of the Poincaré modes also changes with increasing k_x ; see Figs. 2(b) and (c)). The Kelvin and Yanai waves remain localized near the equators. We have also investigated spectra with larger values of U_0 and find that the Kelvin and Yanai waves persist so long as U_0 is not too large. If U_0 is too large, the bulk bands and the boundary modes become difficult to distinguish due to significant changes in the frequency of the bulk modes and the large Doppler shift of the planetary waves, especially in the case of the sine shear flow. We show below that the continued presence of the waves is consistent with the persistence of bulk-interface correspondence in the presence of shear.

B. Bulk waves on the f-plane

We now develop a purely spectral approach to including shear that is amenable to either direct diagonalization or a perturbative expansion. First, we briefly review shallow water waves on the f-plane in the absence of shear flow [1]. We expand the eigenmodes in the plane wave basis, $(u, v, \eta) = \Psi(k_x, k_y, f_0) = \hat{\Psi} \exp(ik_x x + ik_y y - i\omega t)$. In this basis, the linear wave operator is a 3×3 matrix:

$$L_0(k_x, k_y, f_0) = \begin{pmatrix} 0 & if_0 & k_x \\ -if_0 & 0 & k_y \\ k_x & k_y & 0 \end{pmatrix}. \quad (11)$$

The amplitudes of the normal modes $\Psi_{\pm,0}(k_x, k_y, f_0)$ with frequencies $\omega_{\pm,0}$ can be obtained by diagonalizing L_0 . The positive Poincaré mode frequency is $\omega_+ = \sqrt{k_x^2 + k_y^2 + f_0^2}$ with the eigenmode:

$$\Psi_+ = \begin{pmatrix} -\frac{k_x}{k} + i\frac{f_0 k_y}{k\sqrt{k^2 + f_0^2}} \\ \frac{k_y}{k} - i\frac{f_0 k_x}{k\sqrt{k^2 + f_0^2}} \\ \frac{k}{\sqrt{k^2 + f_0^2}} \end{pmatrix}, \quad (12)$$

where $k \equiv \sqrt{k_x^2 + k_y^2}$. A highly degenerate geostrophically-balanced mode appears at zero frequency, $\omega_0 = 0$ (the degeneracy is lifted when the Coriolis parameter varies with latitude or in the presence of shear):

$$\Psi_0(k_x, k_y, f_0) = \frac{1}{\sqrt{k^2 + f_0^2}} \begin{pmatrix} -ik_y \\ ik_x \\ f_0 \end{pmatrix} \quad (13)$$

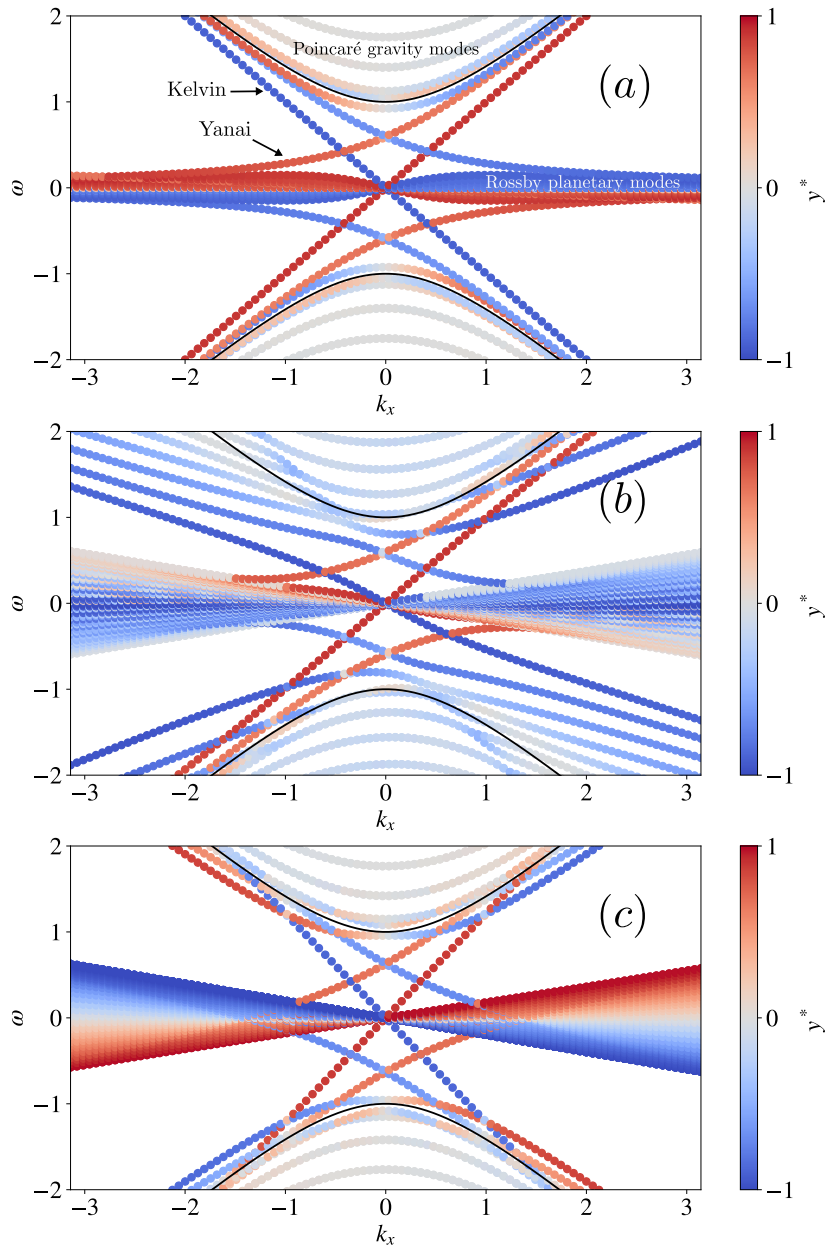


FIG. 2: Numerical evaluation of the frequency-wavenumber dispersion of the linearized shallow water equations obtained with *Dedalus* with $N_y = 61$ spectral modes showing the spectral flow of the Kelvin and Yanai waves between bands. Colors show the projected real space position and $y^* = \langle \Psi | y | \Psi \rangle / L_y$. (a) No shear; (b) Imposed sine shear (Eq. (4)) with $U_0 = 0.2$, and (c) Cosine shear (Eq. (9)) with $U_0 = 0.2$. The Coriolis parameter varies sinusoidally (Eq. (7)) and changes sign at $y = 0$ ($y^* = -1$) and $y = \pm L_y/2$ ($y^* = 1$). We set $L_y = 4\pi$. Black solid lines represent the frequency of the $k_y = 0$ Poincaré modes in the absence of shear and in the f-plane approximation $f = 1$: $\omega = \pm \sqrt{k_x^2 + f^2}$. Colors represent the proximity of the band wavefunctions to the two equators.

Finally the negative Poincaré mode has angular frequency $\omega_- = -\omega_+$ with corresponding wavefunction $\Psi_-(k_x, k_y, f_0) = \Psi_+(-k_x, -k_y, -f_0)$ reflecting the fact that the wave amplitudes in real space are real-valued.

For Poincaré-gravity waves, the gauge-invariant quantity displays a vortex or antivortex (depending on the signs of the frequency and the Coriolis frequency) centered at the origin in wavevector space:

$$\Xi_{\pm}(k_x, k_y) = \frac{k_y - i \operatorname{sgn}(f_0) k_x}{f_0}, \quad (14)$$

where we use the long-wavelength approximation $k^2 \ll f_0^2$. The vortex / antivortex has winding number ± 1 which constitutes its topological charge. Representing the phase of Ξ with an arrow makes these patterns evident as shown in Figure 1. The zero-frequency geostrophic mode, by contrast, has in the same limit

$$\Xi_0(k_x, k_y) = \frac{ik_x}{f_0}, \quad (15)$$

and thus has a domain wall at $k_x = 0$ and zero winding number. Its topological charge therefore vanishes.

C. Horizontal Shear Flow on the f-plane

In the presence of shear flow the system is no longer translationally invariant along the y -direction. While the linear wave operator can still be expressed as a matrix in wavevector space, it is no longer composed of 3×3 block matrices along the diagonal. We first rewrite Eq. (3) in position space in the form of a matrix of differential operators,

$$\hat{L}(x, y, f_0, U_0) = i \begin{pmatrix} U(y)\partial_x & \frac{\partial U(y)}{\partial y} - f_0 & \partial_x \\ f_0 & U(y)\partial_x & \partial_y \\ H(y)\partial_x & H(y)\partial_y - \frac{\partial H}{\partial y} & U(y)\partial_x \end{pmatrix}. \quad (16)$$

This linear operator preserves the parity-time (PT) symmetry despite the broken Hermiticity, and spontaneous PT-symmetry breaking has been known to lead to instabilities [52, 53]. However, note that if the shear flow has dependence on both x and y (i.e., $U(x, y)$), PT symmetry would be broken. Substituting in the sine shear flow $U(y)$ from Eq. (4) with $H(y)$ satisfying the geostrophic balance in Eq. (5), we obtain

$$\hat{L}(x, y, f_0, U_0) = i \begin{pmatrix} U_0 \sin\left(\frac{2\pi y}{\Lambda}\right) \partial_x & \frac{2\pi U_0}{\Lambda} \cos\left(\frac{2\pi y}{\Lambda}\right) - f_0 & \partial_x \\ f_0 & U_0 \sin\left(\frac{2\pi y}{\Lambda}\right) \partial_x & \partial_y \\ \left[1 + \frac{U_0 f_0 \Lambda}{2\pi} \cos\left(\frac{2\pi y}{\Lambda}\right)\right] \partial_x & \left[1 + \frac{U_0 f_0 \Lambda}{2\pi} \cos\left(\frac{2\pi y}{\Lambda}\right)\right] \partial_y - U_0 f_0 \sin\left(\frac{2\pi y}{\Lambda}\right) & U_0 \sin\left(\frac{2\pi y}{\Lambda}\right) \partial_x \end{pmatrix}. \quad (17)$$

Note that the linear wave operator has a y -dependence, which means that when expanding H in wavevector space, different modes with different k_y 's can mix. Without the loss of generality, we assume $\Lambda = 1$. We can consider the simplest case where there are only three modes, $k_y, k_y \pm 2\pi$, in the basis. In this case, the full linear wave operator is a 9×9 matrix that can be decomposed into 3×3 blocks, which can be formally represented as follows,

$$\mathcal{L}_{9 \times 9}(k_x, k_y, f_0, U_0) = \begin{pmatrix} L_0(k_x, k_y + 2\pi, f_0) & T_1(k_x, k_y, f_0, U_0) & 0 \\ T_2(k_x, k_y + 2\pi, f_0, U_0) & L_0(k_x, k_y, f_0) & T_1(k_x, k_y - 2\pi, f_0, U_0) \\ 0 & T_2(k_x, k_y, f_0, U_0) & L_0(k_x, k_y - 2\pi, f_0) \end{pmatrix}, \quad (18)$$

where L_0 is given in Eq. (11) and T_1 and T_2 are the transition matrices between modes:

$$\begin{aligned} T_1(k_x, k_y, f_0, U_0) &= \langle k_x, k_y + 2\pi | \hat{L} | k_x, k_y \rangle \\ &= \frac{U_0}{2} \begin{pmatrix} ik_x & 2\pi i & 0 \\ 0 & ik_x & 0 \\ \frac{f_0 k_x}{2\pi} & \frac{k_y f_0}{2\pi} + f_0 & ik_x \end{pmatrix}, \\ T_2(k_x, k_y, f_0, U_0) &= \langle k_x, k_y - 2\pi | \hat{L} | k_x, k_y \rangle \\ &= \frac{U_0}{2} \begin{pmatrix} -ik_x & 2\pi i & 0 \\ 0 & -ik_x & 0 \\ \frac{f_0 k_x}{2\pi} & \frac{k_y f_0}{2\pi} - f_0 & -ik_x \end{pmatrix}. \end{aligned} \quad (19)$$

The derivation of T_1 and T_2 can be found in Appendix B. The matrix $T_1(k_x, k_y, f_0, U_0)$ connects wavenumber k_y to $k_y + 2\pi$ and $T_2(k_x, k_y, f_0, U_0)$ connects k_y to $k_y - 2\pi$. Note that $T_1 \neq T_2^\dagger$ and the linear wave operator is non-Hermitian. The frequency spectrum and the eigenvectors can then be obtained by diagonalizing the full matrix $\mathcal{L}(k_x, k_y, f_0, U_0)$. We validate our results by comparing our spectra with the ones obtained with *Dedalus* [50] in Appendix C.

D. Perturbative treatment of shear

We also consider a perturbative expansion of the eigenfunctions/values in powers of the shear [54–56]. We may treat the shear flow perturbatively by considering the quantity $\delta\mathcal{L} = \mathcal{L} - \mathcal{L}_0$, namely the off-diagonal blocks in Eq. (18). The correction to the frequency of the Poincaré mode first appears at second order in the shear:

$$\omega_n = \omega_n^{(0)} + \sum_{m \neq n} \frac{\delta\mathcal{L}_{nm}\delta\mathcal{L}_{mn}}{\omega_n^{(0)} - \omega_m^{(0)}}, \quad (20)$$

where $\delta\mathcal{L}_{mn} = \langle m|\delta\mathcal{L}|n\rangle$, and m and n are indices that label a wavevector state with some k_y . The wavefunctions including the first-order correction are given as follows:

$$|n\rangle = |n^{(0)}\rangle + \sum_{m \neq n} \frac{\delta\mathcal{L}_{mn}}{\omega_n^{(0)} - \omega_m^{(0)}} |m^{(0)}\rangle, \quad (21)$$

where $|n^{(0)}\rangle$ and $|m^{(0)}\rangle$ are unperturbed wavefunctions corresponding to some k_y . The perturbed eigenmodes are still labelled by wavevector (k_x, k_y) despite the fact that they contain contributions from modes at other k_y . To second order in the shear U_0 , the frequencies only involve intermediate modes at wavevectors $(k_x, k_y \pm 2\pi)$; higher orders of perturbations involve increasing departures of the wavenumber away from $k_x = 0$. Figure 3 compares the frequency obtained from full diagonalization of the 9×9 linear wave operator to the spectrum from second-order perturbation theory. The two spectra agree well with each other. Through comparing the perturbative spectrum and the full diagonalization, we show that firstly, the bulk can be classified by (k_x, k_y) and secondly, the change of the bulk Poincaré wave is smooth as a function of U_0 . Therefore, we argue that using the bulk-interface correspondence is valid despite the broken Hermiticity. As discussed later in Section VI, the first and second order perturbative corrections to the wavefunctions do not alter their topological properties.

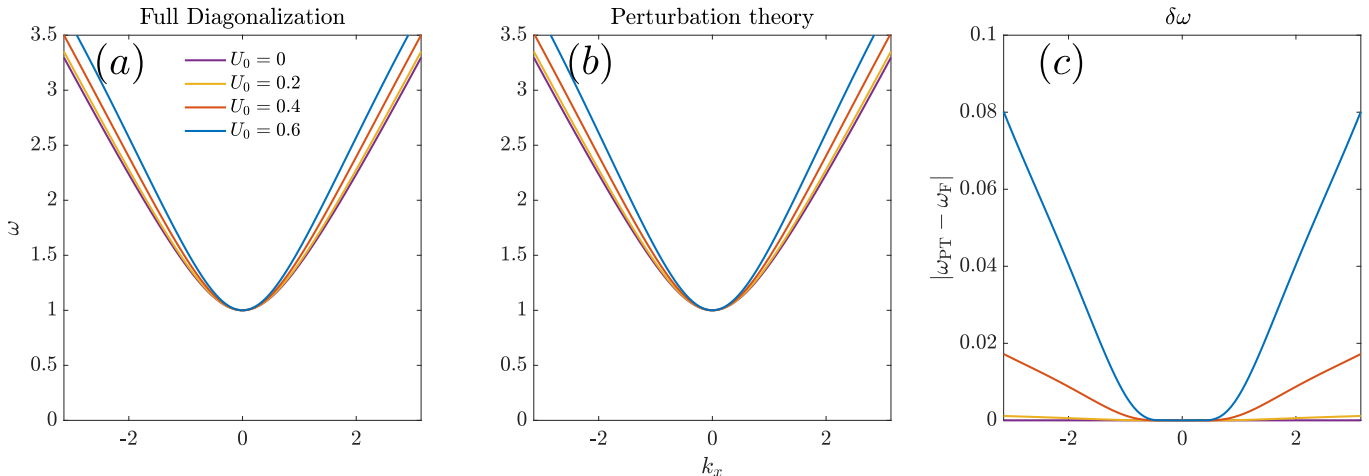


FIG. 3: Comparison of the frequency of the lowest positive frequency Poincaré modes from (a) full diagonalization and (b) perturbation theory of the 9×9 linear wave operator. (c) The difference between the two frequencies in (a) and (b).

E. Wave dynamics

Figures 4 and 5 show snapshots of the propagation of wavenumber 2 ($k_x = 4\pi/L_x$) Kelvin and Yanai waves subjected to sine and cosine shear. The waves remain localized near the $y = 0$ equator as they propagate. The wave amplitude grows in time with the sine shear (Figs. 4 (b) and (d)) and decays in time with the cosine shear (Figs. 5 (b) and (d)), consistent with the imaginary part of the frequency eigenvalues that correspond to growth and decay respectively for the two types of the shear. Note that since the sine shear is odd in y , the Kelvin wave also becomes asymmetric in y as time evolves (Fig. 4(b)).

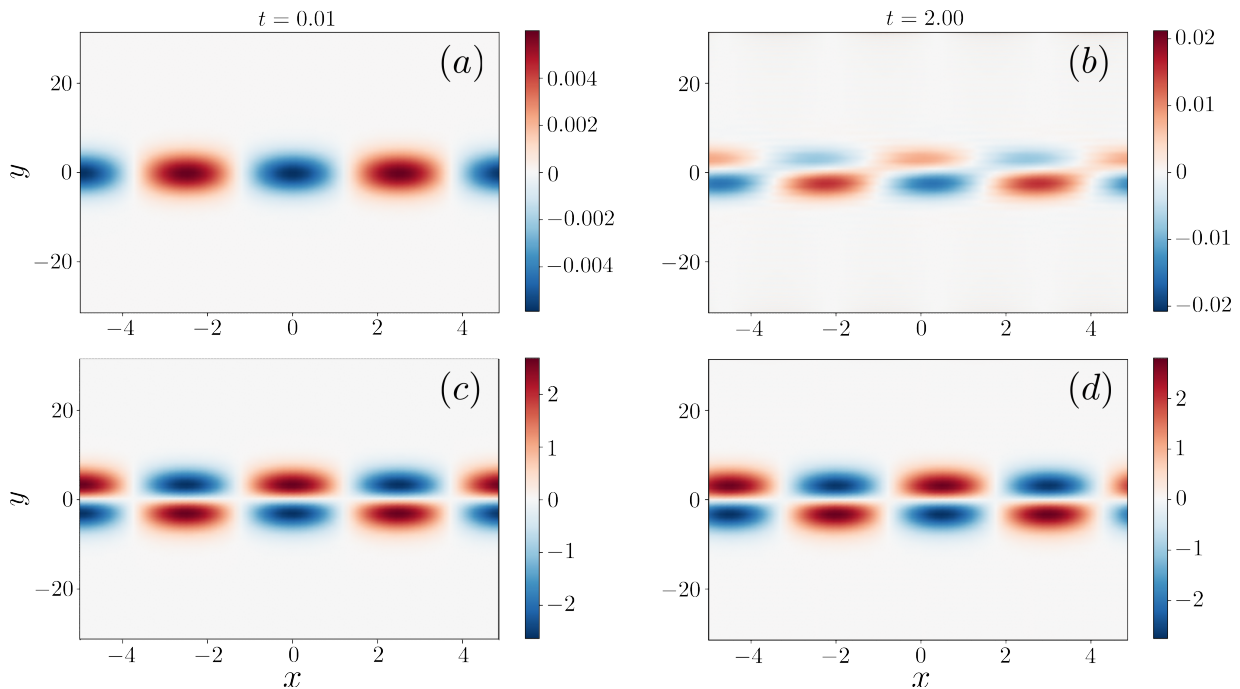


FIG. 4: Time evolution of the η -component of (a, b) the Kelvin wave and (c, d) the Yanai wave for sine shear with $U_0 = 0.1$, $N_y = 121$, $N_x = 71$, $L_y = 20\pi$, $L_x = 10$.

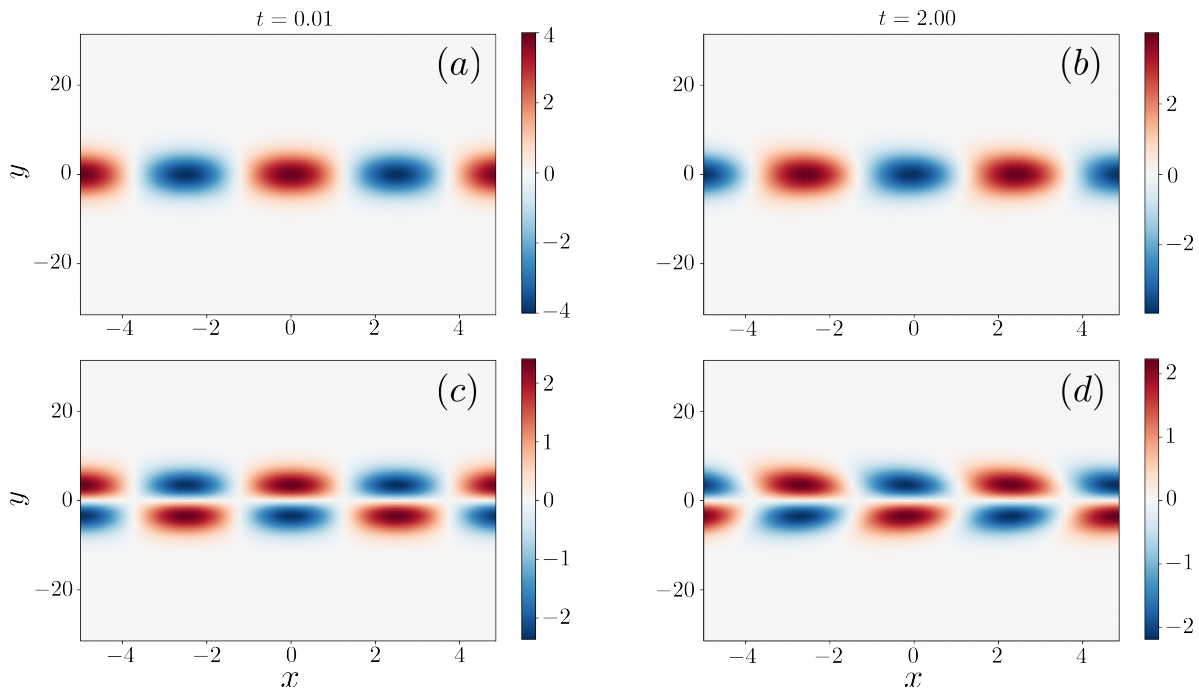


FIG. 5: Time evolution of the η -component of (a, b) the Kelvin wave and (c, d) the Yanai wave for cosine shear with $U_0 = 0.1$, $N_y = 121$, $N_x = 71$, $L_y = 20\pi$, and $L_x = 10$.

IV. PRIMITIVE EQUATIONS WITH AND WITHOUT SHEAR

We turn next to the continuously stratified primitive equations. It has been shown that non-rotating stratified fluids with profiles of stratification that transition with increasing depth from marginally unstable to stable have a wave of topological origin along the interface [57]. We make the standard Boussinesq approximation, and the vertical

velocity or variation in the buoyancy replaces the depth as one of the dynamical fields.

We first analyze the topological character of the linear stratified equations in the absence of shear by calculating the topological invariant within the bulk f-plane approximation. The linearized and non-dimensionalized equations can be derived from the underlying hydrostatic equations (see Appendix D for the detailed derivation):

$$\begin{aligned}\frac{\partial u}{\partial t} &= -U(y)\frac{\partial u}{\partial x} - v\frac{\partial U(y)}{\partial y} + f(y)v - \frac{\partial \eta}{\partial x}, \\ \frac{\partial v}{\partial t} &= -f(y)u - U(y)\frac{\partial v}{\partial x} - \frac{\partial \eta}{\partial y}, \\ \frac{\partial}{\partial t}\frac{\partial \eta}{\partial z} &= -w - U(y)\frac{\partial^2}{\partial x \partial z}\eta,\end{aligned}\tag{22}$$

where w is the vertical velocity and the vertical depth variation η and the buoyancy b are related by the diagnostic relationship $\partial_z \eta = b$.

On the f-plane it is again natural to switch to a basis of plane waves which decouples the modes with different wavenumber in the z-direction, k_z . The incompressibility constraint in this basis takes the form $\nabla \cdot \mathbf{u} = i(k_x u + k_y v + k_z w) = 0$ permitting the replacement of w and η with b , u and v . In the absence of shear, Eq. (22) now corresponds in this basis to the linear wave operator

$$L_0 = \begin{pmatrix} 0 & i f_0 & -i \frac{k_x}{k_z} \\ -i f_0 & 0 & -i \frac{k_y}{k_z} \\ i \frac{k_x}{k_z} & i \frac{k_y}{k_z} & 0 \end{pmatrix}.\tag{23}$$

The eigenfrequencies of Eq. (23) are $\omega_{\pm} = \pm \sqrt{f_0^2 + k^2/k_z^2}$ and $\omega_0 = 0$ with corresponding eigenvectors:

$$\begin{aligned}\Psi_{\pm} &= \frac{1}{\mathcal{N}_1} \begin{pmatrix} \mp i k_z k_x \sqrt{f_0^2 k_z^2 + k^2} + f_0 k_z^2 k_y \\ \mp i k_z k_y \sqrt{f_0^2 k_z^2 + k^2} - f_0 k_z^2 k_x \\ k^2 k_z \end{pmatrix}, \\ \Psi_0 &= \frac{1}{\mathcal{N}_2} \begin{pmatrix} -k_x k_y \\ k_x^2 \\ f_0 k_x k_z \end{pmatrix},\end{aligned}\tag{24}$$

where $k^2 = k_x^2 + k_y^2$, and $\mathcal{N}_{1,2}$ are normalization constants.

We consider the positive frequency eigenvector at fixed non-zero k_z . Letting $f_z = f_0 k_z$ and dividing Ψ_+ by k_z , we have

$$\Psi_{\pm} = \frac{1}{\mathcal{N}_3} \begin{pmatrix} \mp i k_x \sqrt{f_z^2 + k^2} + f_z k_y \\ \mp i k_y \sqrt{f_z^2 + k^2} - f_z k_x \\ k^2 \end{pmatrix},\tag{25}$$

where \mathcal{N}_3 is the new normalization constant. The Berry connection is

$$\text{Im}\langle \Psi_+ | \nabla_{\mathbf{p}} | \Psi_+ \rangle = (-2f_z k_y \sqrt{f_z^2 + k^2}, 2f_z k_x \sqrt{f_z^2 + k^2}, 0),\tag{26}$$

where $\mathbf{p} = (k_x, k_y, f_z)$. The result is the same as the Berry connection of the positive Poincaré mode of the shallow water equations [1]. The difference of the Chern number between the two hemispheres, ΔC_{\pm} , can be calculated analytically by integrating the Berry curvature over the unit sphere in (k_x, k_y, f_z) space. For the Poincaré modes, the difference $\Delta C_{\pm} = \pm 2$. By bulk-interface correspondence, for each k_z , there are two pairs of boundary Kelvin and Yanai modes (one pair each for the two oppositely oriented equators). These stacks of boundary modes are analogous to the edge modes found in weak three-dimensional topological insulators [45].

With sinusoidal horizontal shear flow, the eigenmodes of Eq. (22) can be obtained by the methods outlined in Section III C. The method again shows excellent agreement with the result obtained from *Dedalus* (not shown in the paper).

With a vertical shear flow, the primitive equations are modified to be the following:

$$\begin{aligned}\frac{\partial u}{\partial t} &= -U(z)\frac{\partial u}{\partial x} - f(y)v - \frac{\partial \eta}{\partial x}, \\ \frac{\partial v}{\partial t} &= -f(y)u - U(z)\frac{\partial v}{\partial x} - \frac{\partial \eta}{\partial y}, \\ \frac{\partial}{\partial t}\frac{\partial \eta}{\partial z} &= -w - U(z)\frac{\partial^2 \eta}{\partial x \partial z}.\end{aligned}\tag{27}$$

In this work, we consider a linear vertical shear flow, namely, $U(z) = U_0 z$. We numerically simulated the spectra in the (y, z) space using `Dedaalus` and is shown in Fig. 6 with $U_0 = 0.05$. Similar to Fig. 2, we use a sinusoidal Coriolis parameter $f(y) = \sin(2\pi y/L_y)$ with $L_y = 10\pi$. Both Yanai and Kelvin waves are present at different values of vertical wavenumber k_z .

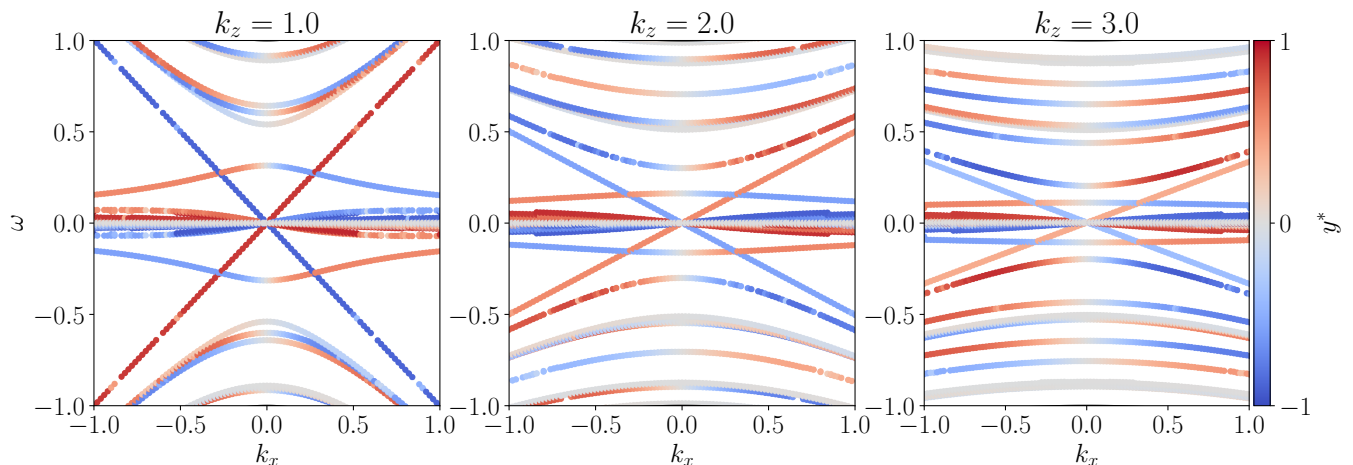


FIG. 6: The spectral flow of Kelvin and Yanai waves between the band gaps exhibited by the linearized primitive equations with a linear vertical shear $U_0 = 0.01$ obtained from `Dedaalus` with $N_y = 24, N_z = 24, L_y = 10\pi, L_z = 2\pi$ using Fourier basis. The vertical wavenumber is (a) $k_z = 1$; (b) $k_z = 2$; and (c) $k_z = 3$. The solid black lines are the dispersion relation for the f -plane approximation with $f = 1$, Eq. (24). As in Fig. 2, the color indicates proximity to the two equators. The missing scattered points are due to the difficulty in separating out the modes that correspond to different vertical wavenumbers k_z .

V. SHEAR INDUCED INSTABILITY

To investigate the stability of the waves in the presence of horizontal shear we follow Ref. [58]. Introducing the background potential vorticity $Q(y) = \frac{f(y) - \partial_y U(y)}{H(y)}$, perturbations are bounded if there exists some constant $\alpha \in \mathbb{R}$ such that the following two conditions hold for all $y \in [-\frac{L_y}{2}, \frac{L_y}{2}]$: (i) $[\alpha - U(y)] \partial_y Q(y) \geq 0$ and $[\alpha - U(y)]^2 \leq H(y)$. For the sine horizontal shear flow condition (ii) can be satisfied, but condition (i) requires that the function $g(U_0, y) = U_0 \sin(2\pi y)$ to be greater or equal to zero over the entire domain, but this condition is violated for any $U_0 \neq 0$. The analysis is similar with a cosine shear. Thus the bulk modes are always unstable in the presence of horizontal shear. We numerically confirm the instability of the bulk modes by presenting the imaginary part of the frequency spectrum in Fig. 7. When $U_0 \neq 0$, the spectrum has a non-zero imaginary part that grows linearly in U_0 for small shear. The instability is most prominent in the planetary Rossby modes.

In the presence of the linear vertical shear with rigid-lid boundaries, since the derivative of $U(z)$ has the same sign at the upper and lower boundaries, Eady instabilities are present at low wavenumbers [5]. We numerically verified the presence of Eady instabilities by simulating the primitive equations and observed that the spectra are unstable at low wavenumbers.

Despite the presence of instabilities with both horizontal and shear flows, the gauge-invariant phase is a robust method of quantifying the topological nature of the system.

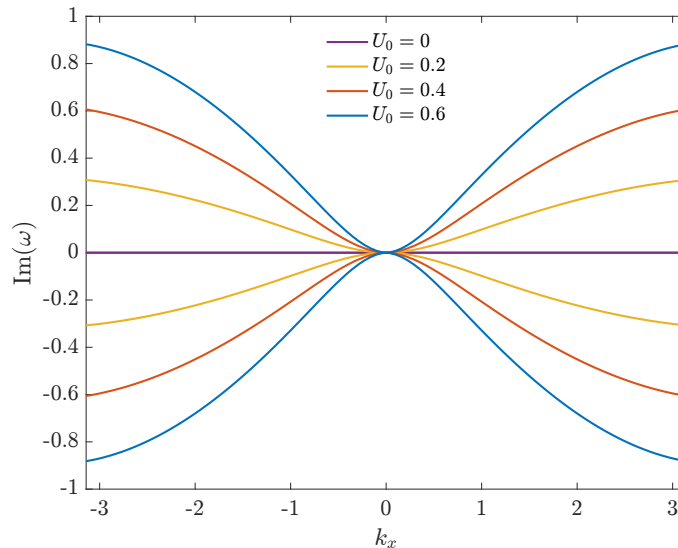


FIG. 7: Imaginary part of the frequency of the lowest-frequency planetary waves obtained from full diagonalization of the 69×69 linear wave operator.

VI. NUMERICAL CALCULATION OF BULK WINDING NUMBERS

For Hermitian systems, bulk-interface correspondence [10, 59] establishes a relationship between the topological invariant, the Chern number of the bulk, and the number of edge modes. It states that the difference in the number of counterpropagating edge modes equals the difference in the Chern number in two bulk regions that are connected at a boundary: $\Delta C = n_L - n_R$, where n_L and n_R are the number of left-moving and right-moving modes. The Chern number can be calculated analytically for the rotating shallow water equations. Each of the 3 bands may be parametrized on the unit (k_x, k_y, f) sphere. The Chern number may then be found by integrating the Berry curvature over the surface of the sphere with a fixed radius $\sqrt{k^2 + f^2}$ [1].

In the presence of shear, however, the linear wave operator is no longer Hermitian, and a rigorous bulk-interface correspondence principle is not in hand. We may still investigate the topological properties of the bulk wavefunctions and compare with the boundary mode spectrum to test whether or not bulk-interface correspondence continues to operate. However, the presence of shear breaks translational invariance in the y -direction and the integral of the Berry curvature becomes difficult to evaluate. As an alternative, we instead look for singularities in the phase of the wavefunctions which appear as vortices in wavevector space [60]. In the context of polarization physics, it has been shown that the winding of the polarization azimuth, or the wavefunction phase, equals the enclosed Chern number [61, 62]. We set the Coriolis parameter such that it is in the bulk (namely, it does not change sign), and examine the phase of the wavefunctions in (k_x, k_y) to check whether there is a vortex or antivortex in the phase.

A. Spatially varying Coriolis parameter

Delplace *et al.* [1] uses an f-plane approximation to analytically calculate the Chern number to show the nontrivial topology of the equatorial waves. However, realistically, Coriolis parameter is a function of the latitude and translational invariance is always broken in the bulk. Here, we first verify that translational invariance in the bulk is not required. To do this we preserve Hermiticity by considering a spatially varying Coriolis parameter in absence of the shear flow and find the winding number of the Poincaré modes. We choose

$$f(y) = f_0 + \Delta f \sin\left(\frac{2\pi y}{L_y}\right), \quad (28)$$

so that we may adapt the formalism introduced in Eq. (18) to write the linear wave operator in wavevector space

with transition blocks:

$$T_1(\Delta f) = \frac{\Delta f}{2} \begin{pmatrix} 0 & 1 & 0 \\ -1 & 0 & 0 \\ 0 & 0 & 0 \end{pmatrix}, \quad T_2(\Delta f) = T_1(k_x, k_y, \Delta f)^T. \quad (29)$$

By diagonalizing the linear wave operator, we can obtain the spectrum of shallow water equations with the y -dependent $f(y)$. We choose Δf and f_0 such that $f(y)$ does not change sign anywhere; thus we remain in the bulk and no edge modes should arise. Figure 8 shows the bulk spectrum with $\Delta f = 0.5$ and $f_0 = 1$. Frequencies obtained by diagonalization (Fig. 8(a)) in wavevector space agree with those obtained with *Dedaalus* (Fig. 8(b)) and confirm that there are no Kelvin or Yanai waves.

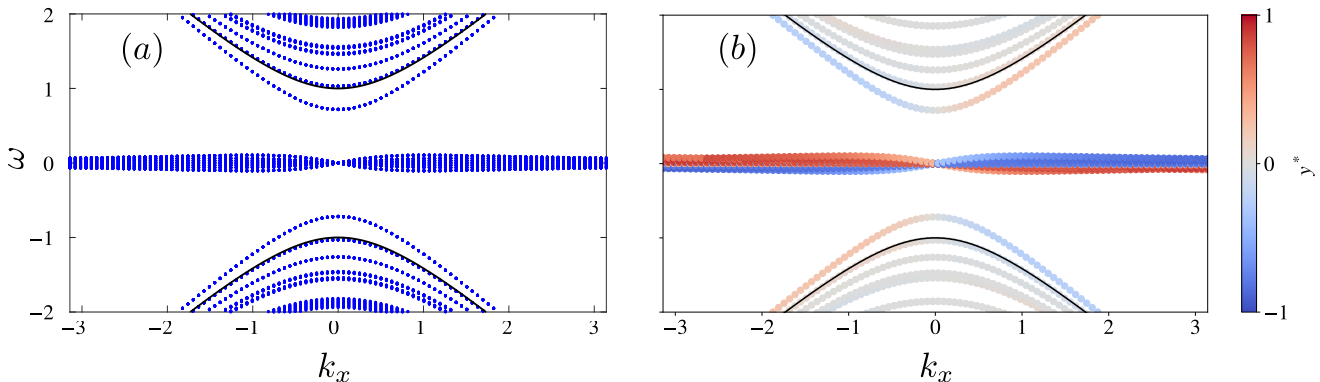


FIG. 8: Numerical calculation of the bulk eigenfrequencies for the spatially varying Coriolis parameter. (a) Diagonalization of the 69×69 wavevector space linear wave operator. (b) *Dedaalus* with $N_y = 23$ for $\Delta f = 0.5$, $f_0 = 1$ and $L = 4\pi$. Black dotted lines in (a) and solid lines in (b) represent the frequency of Poincaré modes in the f-plane approximation with $f_0 = 1$: $\omega = \pm\sqrt{k_x^2 + f_0^2}$. Colors in (b) indicate proximity to the two oppositely oriented equators.

B. Gauge invariant phase

We proceed to calculate the topological index of the bands by searching for singularities in the phase of the frequency eigenfunctions in wavevector space. The eigenfunctions have gauge freedom, as the phase of the three components can be rotated together by an arbitrary amount $\phi(\mathbf{k})$ at each point in wavevector space:

$$\Psi_{\pm,0}(\mathbf{k}) \rightarrow e^{i\phi(\mathbf{k})} \Psi_{\pm,0}(\mathbf{k}). \quad (30)$$

As mentioned previously in Section II we remove the gauge redundancy by multiplying the v -component of the Poincaré modes by the complex conjugate of the η -component, $\eta^*(\mathbf{k}) = \eta(-\mathbf{k})$:

$$\Xi_{\pm}(\mathbf{k}) \equiv v_{\pm}(\mathbf{k}) \eta_{\pm}(-\mathbf{k}) \quad (31)$$

leaving only the internal phase difference between the two amplitudes. Figure 9 depicts the argument of $\Xi_{\pm}(\mathbf{k})$, $\tan^{-1}(\text{Re}(\Xi)/\text{Im}(\Xi))$, of the positive Poincaré modes as a function of k_x and k_y for the spatially varying Coriolis parameter of Eq. (28) where the eigenmodes are obtained by diagonalizing the 69×69 linear operator. The positive Poincaré bands exhibit respectively a vortex and an anti-vortex centered at the origin in wavevector space where the phase cannot be uniquely defined for positive and negative f_0 respectively. The difference in the winding number between the two bands equals 2. The difference in the winding number for either Poincaré band changes by 2 going between the two hemispheres. The planetary waves have no vortex as expected (Fig. 10).

By virtue of the single-valuedness of $\Xi_{\pm}(\mathbf{k})$, the winding number must be integer-valued and thus topological in character. Unlike the calculation of the Chern number which is found by integrating the Berry curvature over wavevector space, no integrals are required for the calculation of the winding number, and the non-compact nature of wavevector space for continuous fluids does not cloud its interpretation.

The Chern number equals the negative of the total winding within a closed domain so $\Delta C = \nu_- - \nu_+$, where ν_{\pm} is the winding number of the positive/negative frequency Poincaré mode and a vortex/anti-vortex corresponds to a

winding number ± 1 [61]. Thus $\Delta C_+ = -2$ for $f_0 > 0$ and $\Delta C_- = 2$ for $f_0 < 0$, in agreement with the Chern numbers found for the f-plane [1]. By bulk-interface correspondence [10, 59], the difference in the number of prograde and retrograde moving edge modes at the equatorial interface where f changes sign equals the change in the Chern number $\{\Delta C_+, \Delta C_0, \Delta C_-\}$, consistent with 2 modes of topological origin localized near each equator. The localized Yanai and Kelvin waves in Fig. 2(a) thus have their origin in topology, just as they do for the shallow water equations using an f-plane approximation. [1].

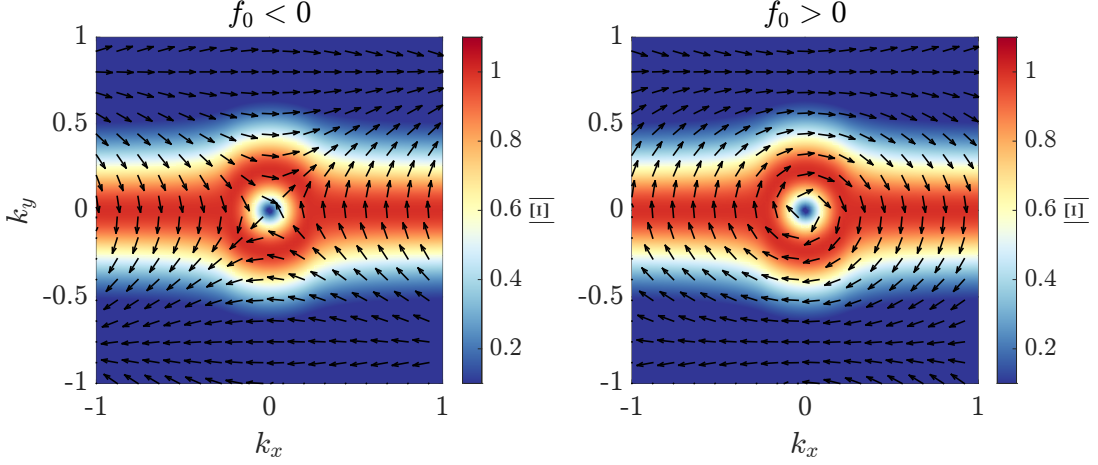


FIG. 9: Arrows representing argument of $\Xi_{\pm}(\mathbf{k}) = v_{\pm}(\mathbf{k})\eta_{\pm}(-\mathbf{k})$ of the lowest positive frequency Poincaré modes as indicated by the direction of the arrows, in the absence of shear but with the sinusoidal Coriolis parameter Eq. (28) with $f_0 = -1$ (left) and $f_0 = 1$ (right), $\Delta f = 0.5$, $\Lambda = 10\pi$, and $L_y \rightarrow \infty$. Colors represent normalized magnitude $|\Xi|$ in arbitrary units.

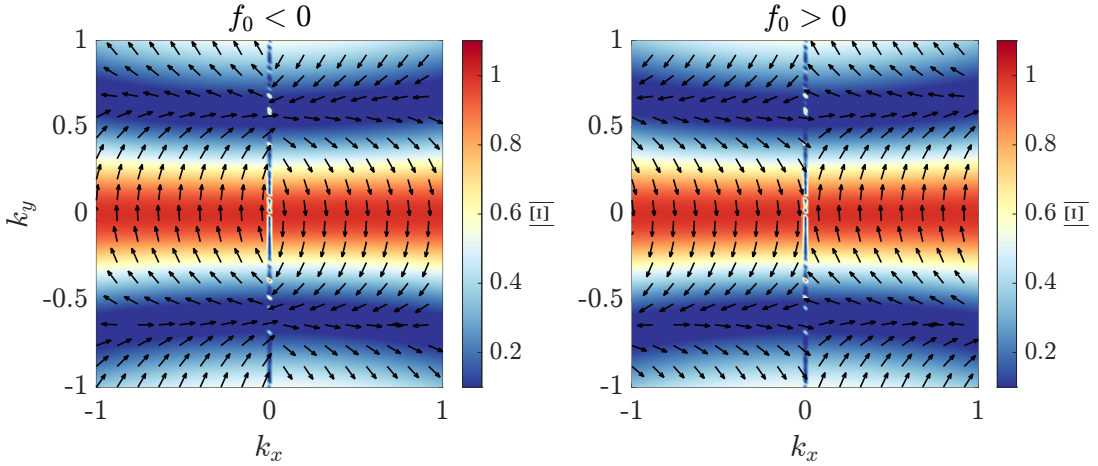


FIG. 10: Arrows representing argument of $\Xi_{\pm}(\mathbf{k}) = v_{\pm}(\mathbf{k})\eta_{\pm}(-\mathbf{k})$ of a Rossby mode as indicated by the direction of the arrows, in the absence of shear but with the sinusoidal Coriolis parameter Eq. (28) with $f_0 = -1$ (left) and $f_0 = 1$ (right), $\Delta f = 0.5$, $\Lambda = 10\pi$, and $L_y \rightarrow \infty$. Colors represent normalized magnitude $|\Xi|$ in arbitrary units. Note that the precise pattern changes depending on which Rossby mode is chosen, but all cases are topologically trivial.

C. Sinusoidal horizontal shear

Next we find the winding number of the Poincaré modes in the shallow water equations subjected to the sinusoidal horizontal shear. Figure 11 shows the phase of $\Xi_{\pm}(\mathbf{k})$ for $U_0 = 0.3$ and constant Coriolis parameter $f_0 = \pm 1$ showing qualitatively similar vortices as those in Fig. 9. Again the positive frequency Poincaré modes exhibit a vortex for $f_0 > 0$ and an anti-vortex for $f_0 < 1$ at the origin in wavevector space (the phase singularity is absent for the planetary modes). The change in the winding number of 2 is consistent with the number of edge modes seen in the spectrum (Fig. 2(b) and (c)). This result suggests that the localized Kelvin and Yanai modes that traverse the gap between

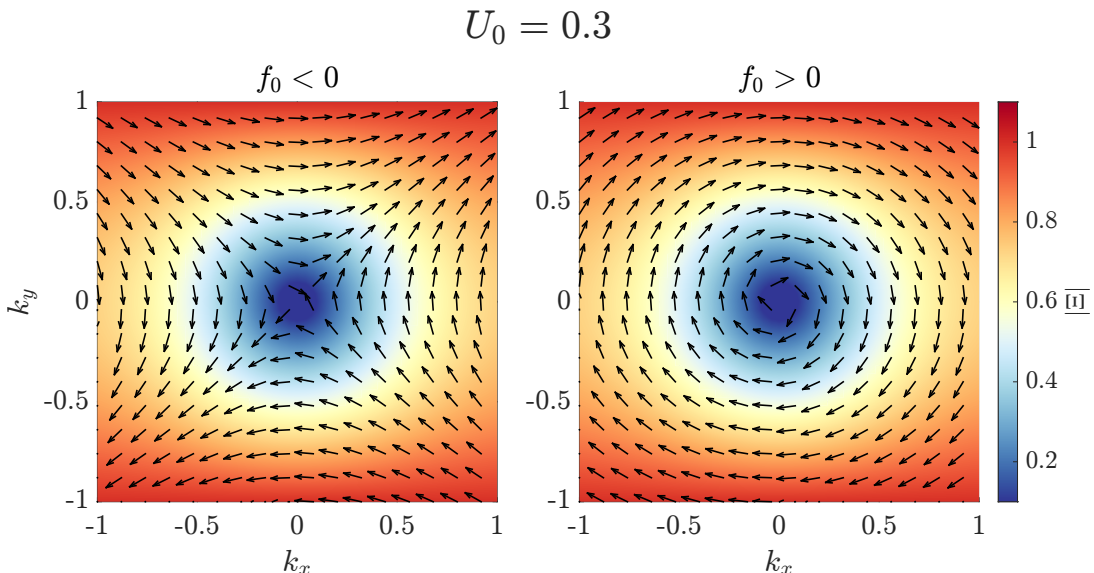


FIG. 11: Arrows representing argument of $\Xi_{\pm}(\mathbf{k}) = v_{\pm}(\mathbf{k})\eta_{\pm}(-\mathbf{k})$ of the lowest positive frequency Poincaré modes as indicated by the direction of the arrows for the case of sinusoidal horizontal shear $U_0 = 0.3$ within the f-plane approximation for $f_0 = -1$ (left) and $f_0 = 1$ (right) with $L_y \rightarrow \infty$. The length of the arrows is rescaled to be equal. Colors represent normalized magnitude $|\Xi|$ in arbitrary units.

Rossby modes and the bulk Poincaré modes have a topological origin like the equatorial modes in the absence of shear. This is the main result of the paper, and we note that the result also holds in perturbation theory with the 9×9 linear wave operator, as the perturbative corrections to the wavefunction do not alter the winding number. The appearance of Kelvin and Yanai waves along the equators shown in Section III A is thus consistent with the persistence of the bulk-interface correspondence in the presence of shear.

Finally, we study the phase of the gauge-invariant quantity $\Xi_{\pm}(\mathbf{k})$ for the linearized primitive equations with and without forcing from sinusoidal horizontal shear. The phase singularity of $\Xi_{\pm}(\mathbf{k})$ for primitive equations (not shown) is similar to that depicted in Figs. 9 and 11. Without shear, the positive and negative frequency Poincaré modes have opposing winding numbers, and the winding number also changes polarity when f changes sign in agreement with the analytic calculation of the Chern number. The vortex of the bulk Poincaré modes continues to be robust in the presence of shear, despite the combined effects of broken translational invariance, non-Hermiticity, and instability. We have verified that the dispersion relation of the shear-forced primitive equations on the planet with two equators continues to exhibit spectral flow of the Kelvin and Yanai waves across the band gaps.

D. Linear vertical shear

We proceed to calculate the winding number of the Poincaré modes in the primitive equators subject to the linear vertical shear flow. Primitive equations with a vertical shear flow $U(z)$ are given as Eq. (27), which we simulate using *DedaLus*. Figure 12 shows that in the presence of linear vertical shear flow, the bulk Poincaré mode exhibits phase singularity, and the winding number depends on the sign of the Coriolis parameters for all vertical wavenumbers k_z 's. This suggests that the Yanai and Kelvin waves in Fig. 6 are topologically nontrivial. Note that while Fig. 12 is obtained with a Fourier basis and thus the effect of the rigid-lid boundary is removed, we verified that the winding numbers are similar to Fig. 12 with a no-slip boundary condition using a Chebyshev basis for each coefficient. Therefore, the topological nature of the boundary waves is robust against the presence of the Eady instability.

VII. DISCUSSION AND CONCLUSION

We investigated the topological properties of rotating shallow water equations and stratified primitive equations in the presence of shear flow that breaks translational invariance in the meridional direction and Hermiticity and introduces instabilities. The winding number of the phase of $\Xi_{\pm}(\mathbf{k})$ serves as a convenient probe of topological properties of the wavefunctions. This alternative to calculating the Chern number remains computationally tractable in the

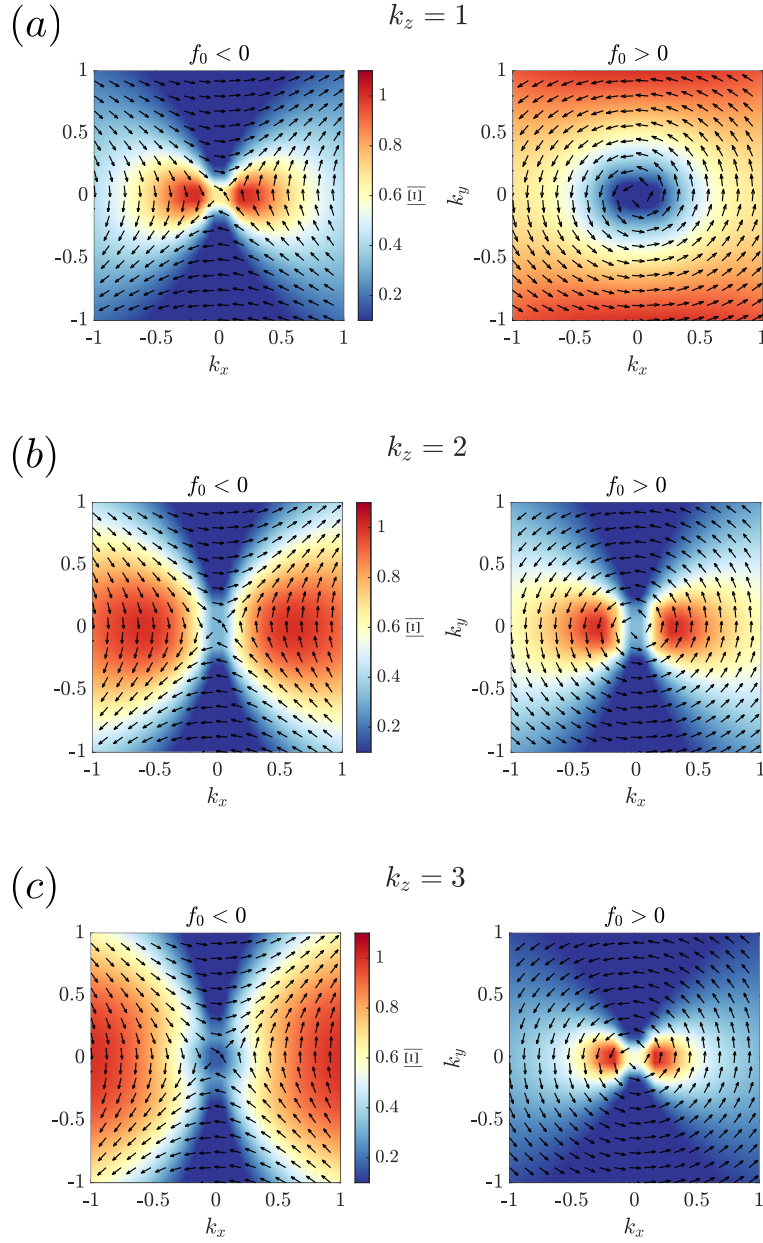


FIG. 12: Arrows representing argument of $\Xi_{\pm}(\mathbf{k}) = v_{\pm}(\mathbf{k})\eta_{\pm}(-\mathbf{k})$ of a positive Poincaré mode as indicated by the direction of the arrows for the case of a linear vertical shear flow with $U_0 = 0.05$ within the f-plane approximation for $f_0 = -1$ (left) and $f_0 = 1$ (right). (a) $k_z = 1$ (b) $k_z = 2$ (c) $k_z = 3$. Colors represent normalized $|\Xi|$ in arbitrary units. Obtained using `Dedaalus` with $N_z = 20$ and $L_z = 2\pi$ using a Fourier basis.

absence of translational invariance and Hermiticity. It may find application to experimental and observational data as well as to idealized theoretical models such as those studied here, as it can be obtained from the (usually neglected) phase information of the cross-periodogram between different fields such as the zonal velocity and geopotential height. To verify that the method yields sensible results, we studied the bulk modes in the presence of a spatially varying Coriolis parameter that does not change sign and demonstrated consistency with the standard calculation of the Chern number on the f-plane [1]. An alternative and equivalent way of quantifying the topological invariant is through the spectral index by counting the number of upward-going eigenvectors for increasing momentum, which is useful when we have access to the wavefunction [46, 63].

Our main result is that the winding number for both the shallow water equations and primitive equations remains

unchanged in the presence of forcing by background shear flow. The difference in the winding number of the Poincaré bands on opposite sides of the equator matches with the number of unidirectional waves localized at the equator, consistent with a topological origin for these forced Kelvin and Yanai waves. For the stratified primitive equations, there are topologically protected modes at each allowed vertical wavenumber in analogy to the physics of weak three-dimensional topological insulators.

We note that we do not rigorously prove the bulk-interface correspondence for the shear flows, nor topological protection. However, we show that the bulk spectrum in f-plane approximation evolves smoothly with increasing U_0 and the phase singularities persist in both the numerically found eigenmodes and in low-order perturbation theory, at least if U_0 is not too large. It may be possible to generalize the approach taken in Ref. [64] for frictionally damped shallow water waves to the problem of background shear. That system, and the problems investigated here, are invariant under the combined operation of parity and time-reversal (PT). We leave this, and an investigation of the maximum shear that will support equatorial waves of topological origin, for future work.

ACKNOWLEDGMENTS

We thank Dan Borgnia, Deven Carmichael, Dung Nguyen, Steve Tobias, and Antoine Venaille for helpful discussions. Z.Z. is supported by the STC Center for Integrated Quantum Materials, NSF Grant No. DMR-1922172, ARO MURI Grant No. W911NF14-0247, NSF DMREF Grant No. 1922165, and a Stanford Science fellowship. J.B.M. is supported in part by a grant from the Simons Foundation (Grant No. 662962, GF) and by U.S. National Science Foundation Grants No. OIA-1921199 and No. OMA-1936221.

Appendix A LINEARIZED SHALLOW WATER EQUATIONS IN THE PRESENCE OF HORIZONTAL SHEAR

We begin with the nonlinear shallow-water equations in the presence of rotation:

$$\begin{aligned} \frac{\partial \mathbf{u}_{\text{tot}}}{\partial t} + (\mathbf{u}_{\text{tot}} \cdot \nabla) \mathbf{u}_{\text{tot}} &= -g \nabla h - \mathbf{f} \times \mathbf{u}_{\text{tot}}, \\ \frac{\partial h}{\partial t} + \nabla \cdot (h \mathbf{u}_{\text{tot}}) &= 0, \end{aligned} \quad (32)$$

where $\mathbf{u}_{\text{tot}} = \mathbf{u} + \mathbf{U}$, $\mathbf{u} = (u, v)$, $\mathbf{U} = (U(y), 0)$ is the shear flow along the zonal direction, $\mathbf{f} = f(y)\hat{z}$ is the Coriolis parameter, and $h = \eta + H(y)$. To the linear order, Eq. (32) can be written as follows,

$$\begin{aligned} \frac{\partial u}{\partial t} + U(y) \frac{\partial u}{\partial x} + v \frac{\partial U(y)}{\partial y} + g \frac{\partial \eta}{\partial x} - f(y)v &= 0, \\ \frac{\partial v}{\partial t} + U(y) \frac{\partial v}{\partial x} + g \frac{\partial \eta}{\partial y} + f(y)u &= 0, \\ \frac{\partial \eta}{\partial t} + H(y) \left(\frac{\partial u}{\partial x} + \frac{\partial v}{\partial y} \right) + v \frac{\partial H(y)}{\partial y} + U(y) \frac{\partial \eta}{\partial x} &= 0. \end{aligned} \quad (33)$$

A deformation length scale L_d and gravity wave speed c are defined to be:

$$L_d \equiv \frac{c}{2\Omega}, \quad c \equiv \sqrt{gH}, \quad (34)$$

where H is the zonally averaged depth without shear ($H(y) = H + h(y)$). Introducing the dimensionless quantities $\tilde{t} = 2\Omega t$, $\tilde{\eta} = \frac{\eta}{H}$, $\tilde{H}(y) = 1 + \frac{h(y)}{H}$, $\tilde{\mathbf{u}} = \frac{\mathbf{u}}{c}$, $\tilde{\mathbf{U}} = \frac{\mathbf{U}}{c}$, $\tilde{f}(y) = \frac{f(y)}{2\Omega}$, and $\tilde{\mathbf{x}} = \frac{\mathbf{x}}{L_d}$, the linearized equations of motion (Eq. (33)) around the basic state ($\mathbf{u} = 0, h = H$) can then be written as follows:

$$\begin{aligned} \partial_{\tilde{t}} \tilde{u} + \tilde{U}(y) \partial_{\tilde{x}} \tilde{u} + \tilde{v} \partial_{\tilde{y}} \tilde{U}(y) + \partial_{\tilde{x}} \tilde{\eta} - \tilde{f}(y) \tilde{v} &= 0, \\ \partial_{\tilde{t}} \tilde{v} + \tilde{U}(y) \partial_{\tilde{x}} \tilde{v} + \partial_{\tilde{y}} \tilde{\eta} + \tilde{f}(y) \tilde{u} &= 0, \\ \partial_{\tilde{t}} \tilde{\eta} + \tilde{H}(y) (\partial_{\tilde{x}} \tilde{u} + \partial_{\tilde{y}} \tilde{v}) + \tilde{v} \partial_{\tilde{y}} \tilde{H}(y) + \tilde{U}(y) \partial_{\tilde{x}} \tilde{\eta} &= 0. \end{aligned} \quad (35)$$

For convenience, we drop the tilde in the main text.

Appendix B THE SHALLOW WATER LINEAR WAVE OPERATOR IN WAVEVECTOR SPACE

The matrix elements of the linear wave operator Eq. (16) in wavevector space may be written using Dirac bracket notation as $\langle k'_x, k'_y | \hat{L} | k_x, k_y \rangle$. Since the linear wave operator has no dependence on x these matrix elements are non-zero only for $k'_x = k_x$. Along the y -direction, we make use of the following relations,

$$\frac{1}{L_y} \int_{-L_y/2}^{L_y/2} dy \sin\left(\frac{2\pi y}{L_y}\right) e^{i(k'_y - k_y)y} = \frac{1}{2i} \left[\delta_{k'_y, k_y - 2\pi/L_y} - \delta_{k'_y, k_y + 2\pi/L_y} \right], \quad (36)$$

and

$$\frac{1}{L_y} \int_{-L_y/2}^{L_y/2} dy \cos\left(\frac{2\pi y}{L_y}\right) e^{i(k'_y - k_y)y} = \frac{1}{2} \left[\delta_{k'_y, k_y - 2\pi/L_y} + \delta_{k'_y, k_y + 2\pi/L_y} \right]. \quad (37)$$

In the absence of shear ($U_0 = 0$), the linear wave operator in k -space is a block-diagonal matrix, with the diagonal blocks being $L_0(k_x, k_y, f)$ and with no off-diagonal blocks. The 3×3 linear wave operators L_0 at wavevectors (k_x, k_y) and $(k_x, k_y \pm 2\pi)$ are connected by the sinusoidal horizontal shear as a wave at wavevector k_y mixes with modes $k'_y = k_y \pm 2\pi$. For a given k_x , we need to diagonalize the full matrix in the basis of $k_y, k_y \pm 2\pi, k_y \pm 4\pi, \dots$ imposing a finite cutoff in $|k'_y|$ to keep the dimension of the matrix finite.

Appendix C COMPARISON WITH DEDALUS

We validate our diagonalization scheme by comparing with *Dedalus* [50]. Figure 13 compares the spectra from diagonalizing a 69×69 linear wave operator corresponding to the 23 retained wavevectors in the y -direction with the spectrum obtained from *Dedalus*. To enable the comparison, the linear wave operator has been truncated to finite dimension in wavenumber space to match the total number of equations in *Dedalus*. The full diagonalization captures both the spread of the geostrophic modes and the bulk Poincaré modes. Note that the small difference in the geostrophic modes is due to the fact that the sample points along the y -direction in *Dedalus* is non-uniform whereas in the direct diagonalization, k_y 's are sampled uniformly. Figure 14 compares the positive frequency modes obtained from full diagonalization versus those found using *Dedalus*. The two methods show an excellent agreement. The frequency of the Poncaré modes increases with increasing shear and remain distinct beyond $U_0 = 0.6$. We can apply the same procedure to obtain the transition matrices T_1 and T_2 for the cosine shear, and the spectra agrees with Figs. 13 and 14, as expected.

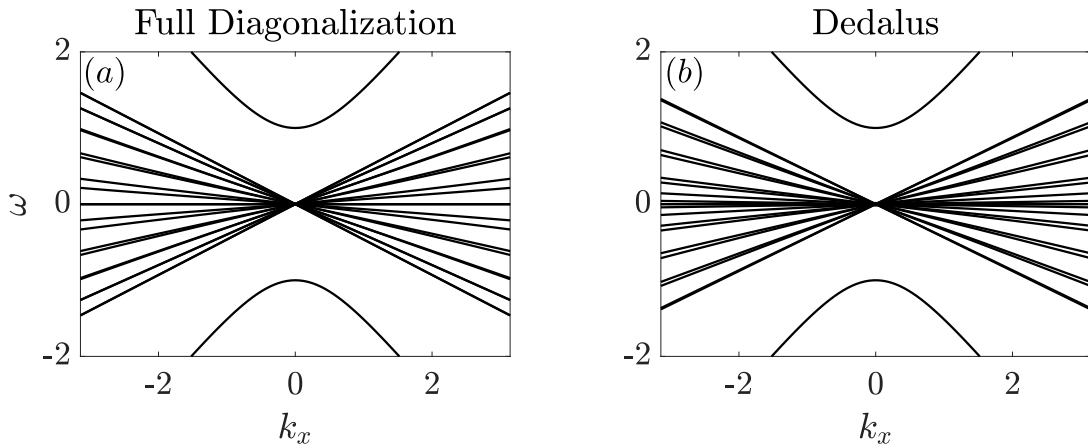


FIG. 13: Frequency spectra of the shallow water equations in the f-plane approximation with $f = 1$ and subjected to sine shear $U_0 = 0.5$. The frequencies are obtained by (a) diagonalizing the 69×69 wavevector space linear wave operator and from (b) *Dedalus* with $N_y = 23$.

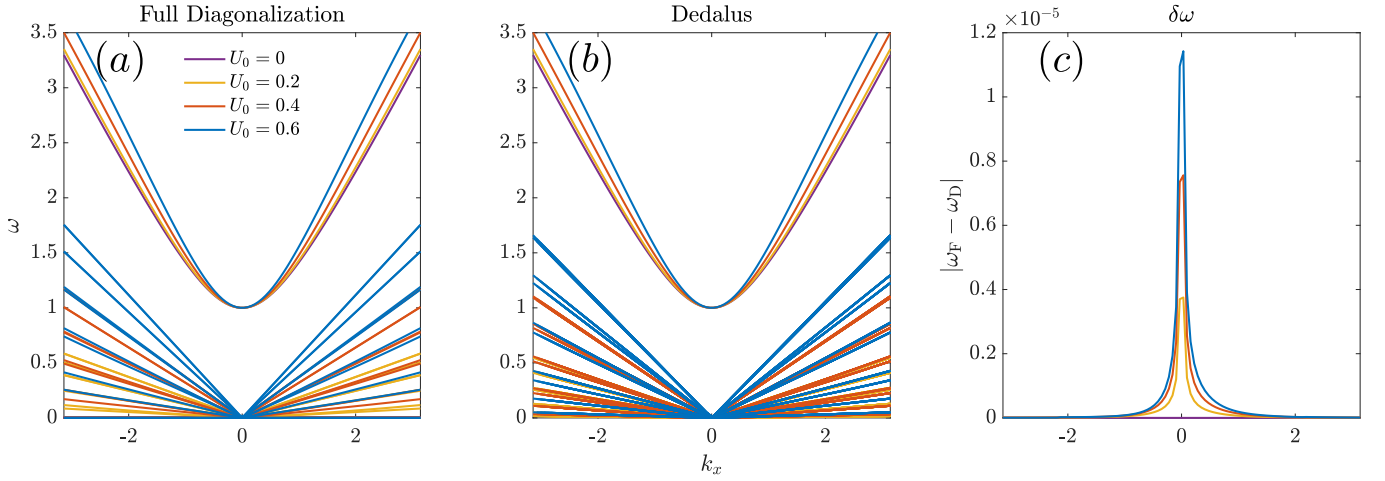


FIG. 14: Comparison of the frequencies of the positive Poincaré and planetary modes. (a) Full diagonalization of the 69×69 linear wave operator. (b) **Dedalus** with $N_y = 23$. (c) The difference between frequencies of the lowest positive Poincaré mode obtained from full diagonalization, ω_F , and Dedalus, ω_D in (a) and (b).

Appendix D PRIMITIVE EQUATIONS

Using the same non-dimensionalization as Appendix A, the non-dimensional Boussinesq primitive equations are given as follows [5]:

$$\begin{aligned}
 R_0 \frac{D\mathbf{u}}{Dt} + \mathbf{f}(y) \times \mathbf{u} &= -\nabla\phi, \\
 R_0 \frac{Db}{Dt} + \left(\frac{L_d}{L_y}\right)^2 N^2 w &= 0 \\
 \partial_z \phi &= b, \\
 \partial_x u + \partial_y v + \partial_z w &= 0.
 \end{aligned} \tag{38}$$

where w is the vertical velocity, ϕ is the kinetic pressure, and b is the buoyancy fluctuation about an average stratification, $N^2 = \partial b / \partial z$, and L_d is the deformation radius, and R_0 is the Rossby number. We consider the linearized equations

$$\begin{aligned}
 R_0 \frac{\partial \mathbf{u}}{\partial t} + \mathbf{f}(y) \times \mathbf{u} &= -\nabla\phi, \\
 R_0 \frac{\partial b}{\partial t} + \left(\frac{L_d}{L_y}\right)^2 N^2 w &= 0, \\
 \partial_z \phi &= b, \\
 \partial_x u + \partial_y v + \partial_z w &= 0.
 \end{aligned} \tag{39}$$

Here, R_0 and NL_d/L_y can be set to unity by appropriate re-scaling of the variables. In the Fourier space, $-ik_z \phi = b$ and $ik_x u + ik_y v + ik_z w = 0$. Therefore, we can eliminate ϕ and w by writing them in terms of b , u and v . In the f-plane approximation, the dispersion relation for the Poincaré modes is $\omega^2 = f^2 + (k_x^2 + k_y^2)/k_z^2$.

Finally we consider the imposition of sinusoidal horizontal shear flow. We assume the system is periodic in the zonal and meridional direction and has rigid lids at $z = 0$ and $z = L_z$, where L_z is a constant. Let $\mathbf{u}_{\text{tot}} = \mathbf{u} + \mathbf{U}$, $\mathbf{u} = (u, v)$, $\mathbf{U} = (U(y), 0)$ and $\phi = \eta + H(y)$. From geostrophic balance, $U(y)$ and $H(y)$ must satisfy Eq. (5). Substituting \mathbf{u}_{tot}

and ϕ into Eq. (38) and discarding non-linear terms, we obtain:

$$\begin{aligned}\frac{\partial u}{\partial t} &= -U(y)\frac{\partial u}{\partial x} - v\frac{\partial U(y)}{\partial y} + \frac{f(y)}{R_0}v - \frac{1}{R_0}\frac{\partial \eta}{\partial x}, \\ \frac{\partial v}{\partial t} &= -\frac{f(y)}{R_0}u - U(y)\frac{\partial v}{\partial x} - \frac{1}{R_0}\frac{\partial \eta}{\partial y}, \\ \frac{\partial}{\partial t}\frac{\partial \eta}{\partial z} &= -\frac{1}{R_0}\left(\frac{L_d}{L_y}\right)^2 N^2 w - U(y)\frac{\partial^2}{\partial x \partial z}\eta.\end{aligned}\quad (40)$$

Again R_0 and $N^2(L_d/L_y)^2$ may be set to unity. By doing so, Eq. (40) simplifies to

$$\begin{aligned}\frac{\partial u}{\partial t} &= -U(y)\frac{\partial u}{\partial x} - v\frac{\partial U(y)}{\partial y} + f(y)v - \frac{\partial \eta}{\partial x}, \\ \frac{\partial v}{\partial t} &= -f(y)u - U(y)\frac{\partial v}{\partial x} - \frac{\partial \eta}{\partial y}, \\ \frac{\partial}{\partial t}\frac{\partial \eta}{\partial z} &= -w - U(y)\frac{\partial^2}{\partial x \partial z}\eta.\end{aligned}\quad (41)$$

-
- [1] P. Delplace, J. B. Marston, and A. Venaille, Topological origin of equatorial waves, *Science* **358**, 1075 (2017).
- [2] A. Venaille and P. Delplace, Wave topology brought to the coast, *Physical Review Research* **3**, 043002 (2021), 2011.03440.
- [3] W. Thomson, On Gravitational Oscillations of Rotating Water, *Proceedings of the Royal Society of Edinburgh* **10**, 92 (1880).
- [4] W. Xu, B. Fox-Kemper, J.-E. Lee, J. Marston, and Z. Zhu, Topological signature of stratospheric poincare–gravity waves, arXiv preprint arXiv:2306.12191 (2023).
- [5] G. K. Vallis, *Atmospheric and Oceanic Fluid Dynamics, Second Edition* (Cambridge University Press, Cambridge, UK, 2017).
- [6] M. Hammond and R. T. Pierrehumbert, Wave-mean Flow Interactions in the Atmospheric Circulation of Tidally Locked Planets, *The Astrophysical Journal* **869**, 0 (2019).
- [7] W. V. R. Malkus, Outline of a theory of turbulent shear flow, *Journal of Fluid Mechanics* **1**, 521 (1956).
- [8] B. D. Fried, M. Gell-Mann, J. D. Jackson, and H. W. Wyld, Longitudinal plasma oscillations in an electric field, *Journal of Nuclear Energy. Part C, Plasma Physics, Accelerators, Thermonuclear Research* **1**, 190 (1960).
- [9] J. R. Herring, Investigation of Problems in Thermal Convection., *Journal of Atmospheric Sciences* **20**, 325 (1963-07).
- [10] M. Z. Hasan and C. L. Kane, Colloquium: Topological insulators, *Rev. Mod. Phys.* **82**, 3045 (2010).
- [11] X.-L. Qi and S.-C. Zhang, Topological insulators and superconductors, *Reviews of Modern Physics* **83**, 1057 (2011), arXiv:1008.2026 [cond-mat.mes-hall].
- [12] Z. Wang, Y. Chong, J. D. Joannopoulos, and M. Soljačić, Observation of unidirectional backscattering-immune topological electromagnetic states, *Nature (London)* **461**, 772 (2009).
- [13] Y. Plotnik, M. C. Rechtsman, D. Song, M. Heinrich, J. M. Zeuner, S. Nolte, Y. Lumer, N. Malkova, J. Xu, A. Szameit, Z. Chen, and M. Segev, Observation of unconventional edge states in ‘photonic graphene’, *Nature Materials* **13**, 57 (2014), arXiv:1210.5361 [cond-mat.mes-hall].
- [14] S. A. Skirlo, L. Lu, and M. Soljačić, Multimode One-Way Waveguides of Large Chern Numbers, *Phys. Rev. Lett.* **113**, 113904 (2014).
- [15] S. A. Skirlo, L. Lu, Y. Igarashi, Q. Yan, J. Joannopoulos, and M. Soljačić, Experimental Observation of Large Chern Numbers in Photonic Crystals, *Phys. Rev. Lett.* **115**, 253901 (2015), arXiv:1504.04399 [physics.optics].
- [16] V. Peano, C. Brendel, M. Schmidt, and F. Marquardt, Topological Phases of Sound and Light, *Physical Review X* **5**, 031011 (2015), arXiv:1409.5375 [cond-mat.mes-hall].
- [17] Z. Yang, F. Gao, X. Shi, X. Lin, Z. Gao, Y. Chong, and B. Zhang, Topological acoustics, *Phys. Rev. Lett.* **114**, 114301 (2015).
- [18] C. He, X. Ni, H. Ge, X.-C. Sun, Y.-B. Chen, M.-H. Lu, X.-P. Liu, and Y.-F. Chen, Acoustic topological insulator and robust one-way sound transport, *Nat. Phys.* **12**, 1124 (2016).
- [19] L. M. Nash, D. Kleckner, A. Read, V. Vitelli, A. M. Turner, and W. T. M. Irvine, Topological mechanics of gyroscopic metamaterials, *Proceedings of the National Academy of Science* **112**, 14495 (2015), arXiv:1504.03362 [cond-mat.soft].
- [20] S. D. Huber, Topological mechanics, *Nature Physics* **12**, 621 (2016).
- [21] M. G. Silveirinha, Chern invariants for continuous media, *Phys. Rev. B* **92**, 125153 (2015).
- [22] S. Shankar, M. J. Bowick, and M. C. Marchetti, Topological sound and flocking on curved surfaces, *Phys. Rev. X* **7**, 031039 (2017).
- [23] R. Green, J. Armas, J. de Boer, and L. Giomi, Topological waves in passive and active fluids on curved surfaces: a unified

- picture, arXiv e-prints , arXiv:2011.12271 (2020), [arXiv:2011.12271 \[cond-mat.soft\]](#).
- [24] J. B. Parker, J. B. Marston, S. M. Tobias, and Z. Zhu, Topological Gaseous Plasmon Polariton in Realistic Plasma, *Phys. Rev. Lett.* **124**, 195001 (2020), [arXiv:1911.01069 \[physics.plasm-ph\]](#).
- [25] J. B. Parker, J. W. Burby, J. B. Marston, and S. M. Tobias, Nontrivial topology in the continuous spectrum of a magnetized plasma, *Physical Review (Series I)* **2**, 033425 (2020).
- [26] Y. Fu and H. Qin, Topological phases and bulk-edge correspondence of magnetized cold plasmas, *Nature Communications* **12**, 3924 (2021), [arXiv:2012.13611 \[physics.plasm-ph\]](#).
- [27] Y. E. Kraus, Y. Lahini, Z. Ringel, M. Verbin, and O. Zilberberg, Topological States and Adiabatic Pumping in Quasicrystals, *Phys. Rev. Lett.* **109**, 106402 (2012), [arXiv:1109.5983 \[cond-mat.mes-hall\]](#).
- [28] M. Lohse, C. Schweizer, O. Zilberberg, M. Aidelsburger, and I. Bloch, A Thouless quantum pump with ultracold bosonic atoms in an optical superlattice, *Nature Physics* **12**, 350 (2016), [arXiv:1507.02225 \[cond-mat.quant-gas\]](#).
- [29] M. A. Bandres, S. Wittek, G. Harari, M. Parto, J. Ren, M. Segev, D. N. Christodoulides, and M. Khajavikhan, Topological insulator laser: Experiments, *Science* **359**, 10.1126/science.aar4005 (2018).
- [30] O. Zilberberg, S. Huang, J. Guglielmon, M. Wang, K. P. Chen, Y. E. Kraus, and M. C. Rechtsman, Photonic topological boundary pumping as a probe of 4D quantum Hall physics, *Nature (London)* **553**, 59 (2018).
- [31] R. P. Pedro, J. Paulose, A. Souslov, M. Dresselhaus, and V. Vitelli, Topological Protection Can Arise from Thermal Fluctuations and Interactions, *Phys. Rev. Lett.* **122**, 118001 (2019), [arXiv:1803.04951 \[cond-mat.soft\]](#).
- [32] H. Shen, B. Zhen, and L. Fu, Topological Band Theory for Non-Hermitian Hamiltonians, *Phys. Rev. Lett.* **120**, 146402 (2018), [arXiv:1706.07435 \[cond-mat.mes-hall\]](#).
- [33] Z. Gong, Y. Ashida, K. Kawabata, K. Takasan, S. Higashikawa, and M. Ueda, Topological Phases of Non-Hermitian Systems, *Physical Review X* **8**, 031079 (2018), [arXiv:1802.07964 \[cond-mat.mes-hall\]](#).
- [34] H. Zhou and J. Y. Lee, Periodic table for topological bands with non-Hermitian symmetries, *Phys. Rev. B* **99**, 235112 (2019), [arXiv:1812.10490 \[cond-mat.mes-hall\]](#).
- [35] D. S. Borgnia, A. J. Kruchkov, and R.-J. Slager, Non-Hermitian Boundary Modes and Topology, *Phys. Rev. Lett.* **124**, 056802 (2020), [arXiv:1902.07217 \[cond-mat.mes-hall\]](#).
- [36] T. E. Lee, Anomalous Edge State in a Non-Hermitian Lattice, *Phys. Rev. Lett.* **116**, 133903 (2016), [arXiv:1603.05312 \[quant-ph\]](#).
- [37] Y. Xiong, Why does bulk boundary correspondence fail in some non-hermitian topological models, *Journal of Physics Communications* **2**, 035043 (2018), [arXiv:1705.06039 \[cond-mat.mes-hall\]](#).
- [38] S. Yao and Z. Wang, Edge States and Topological Invariants of Non-Hermitian Systems, *Phys. Rev. Lett.* **121**, 086803 (2018), [arXiv:1803.01876 \[cond-mat.mes-hall\]](#).
- [39] F. K. Kunst, E. Edvardsson, J. C. Budich, and E. J. Bergholtz, Biorthogonal Bulk-Boundary Correspondence in Non-Hermitian Systems, *Phys. Rev. Lett.* **121**, 026808 (2018), [arXiv:1805.06492 \[cond-mat.mes-hall\]](#).
- [40] C. Yin, H. Jiang, L. Li, R. Lü, and S. Chen, Geometrical meaning of winding number and its characterization of topological phases in one-dimensional chiral non-Hermitian systems, *Phys. Rev. A* **97**, 052115 (2018), [arXiv:1802.04169 \[cond-mat.mes-hall\]](#).
- [41] T. Helbig, T. Hofmann, S. Imhof, M. Abdelghany, T. Kiessling, L. W. Molenkamp, C. H. Lee, A. Szameit, M. Greiter, and R. Thomale, Generalized bulk-boundary correspondence in non-Hermitian topoelectrical circuits, *Nature Physics* **16**, 747 (2020), [arXiv:1907.11562 \[cond-mat.mes-hall\]](#).
- [42] L. Xiao, T. Deng, K. Wang, G. Zhu, Z. Wang, W. Yi, and P. Xue, Non-Hermitian bulk-boundary correspondence in quantum dynamics, *Nature Physics* **16**, 761 (2020), [arXiv:1907.12566 \[cond-mat.mes-hall\]](#).
- [43] A. Ghatak, M. Brandenbourger, J. van Wezel, and C. Coulais, Observation of non-Hermitian topology and its bulk-edge correspondence in an active mechanical metamaterial, *Proceedings of the National Academy of Science* **117**, 29561 (2020), [arXiv:1907.11619 \[cond-mat.mes-hall\]](#).
- [44] D. J. Thouless, M. KOHMOTO, M. P. NIGHTINGALE, and M. DENNIJS, Quantized Hall Conductance in a Two-Dimensional Periodic Potential, *Physical Review Letters* **49**, 405 (1982).
- [45] M. Z. Hasan and J. E. Moore, Three-Dimensional Topological Insulators, *Annual Review of Condensed Matter Physics* **2**, 55 (2011), [arXiv:1011.5462 \[cond-mat.str-el\]](#).
- [46] F. Faure, Manifestation of the topological index formula in quantum waves and geophysical waves, arXiv **math-ph** (2019).
- [47] J. B. Parker, Topological phase in plasma physics, *Journal of Plasma Physics* **87**, 835870202 (2021).
- [48] S. A. R. Horsley, Tutorial: Topology, waves, and the refractive index, arXiv:2202.08643 [10.48550/arxiv.2202.08643](#) (2022), [2202.08643](#).
- [49] O. Bühler, *Waves and mean flows* (Cambridge University Press, 2014).
- [50] K. J. Burns, G. M. Vasil, J. S. Oishi, D. Lecoanet, and B. P. Brown, Dedalus: A flexible framework for numerical simulations with spectral methods, Submitted. [arXiv:1905.10388](#) (2019).
- [51] G. Brunet and T. Warn, Rossby Wave Critical Layers on a Jet., *Journal of Atmospheric Sciences* **47**, 1173 (1990).
- [52] Y. Fu and H. Qin, The physics of spontaneous parity-time symmetry breaking in the Kelvin-Helmholtz instability, *New Journal of Physics* **22**, 083040 (2020), [arXiv:2002.12279 \[physics.plasm-ph\]](#).
- [53] T. W. David, P. Delplace, and A. Venaille, How do CPT-like symmetries shape the stability of geophysical flows?, arXiv e-prints , [arXiv:2112.09511](#) (2021), [arXiv:2112.09511 \[physics.ao-ph\]](#).
- [54] M. M. Sternheim and J. F. Walker, Non-Hermitian Hamiltonians, Decaying States, and Perturbation Theory, *Phys. Rev. C* **6**, 114 (1972).
- [55] C. Buth, R. Santra, and L. S. Cederbaum, Non-Hermitian Rayleigh-Schrödinger perturbation theory, *Phys. Rev. A* **69**, 032505 (2004), [arXiv:physics/0401081 \[physics.chem-ph\]](#).

- [56] J. P. Boyd, The effects of latitudinal shear on equatorial waves. part i: Theory and methods, *Journal of Atmospheric Sciences* **35**, 2236 (1978).
- [57] M. Perrot, P. Delplace, and A. Venaille, Topological transition in stratified fluids, *Nature (London)* **15**, 781 (2019).
- [58] P. Ripa, General stability conditions for zonal flows in a one-layer model on the beta-plane or the sphere, *Journal of Fluid Mechanics* **126**, 463 (1983).
- [59] Y. Hatsugai, Chern number and edge states in the integer quantum Hall effect, *Phys. Rev. Lett.* **71**, 3697 (1993).
- [60] Z. F. Wang, K.-H. Jin, and F. Liu, Quantum spin Hall phase in 2D trigonal lattice, *Nature Communications* **7**, 12746 (2016).
- [61] T. Fösel, V. Peano, and F. Marquardt, L lines, C points and Chern numbers: understanding band structure topology using polarization fields, *New Journal of Physics* **19**, 115013 (2017), [arXiv:1703.08191](https://arxiv.org/abs/1703.08191) [cond-mat.mes-hall].
- [62] P. Bouteyre, D. X. Nguyen, G. Gachon, T. Benyattou, X. Letartre, P. Viktorovitch, S. Callard, L. Ferrier, and H. S. Nguyen, Non-Hermitian topological invariant of photonic band structures undergoing inversion, [arXiv:2211.09884](https://arxiv.org/abs/2211.09884) (2022), [2211.09884](https://arxiv.org/abs/2211.09884).
- [63] A. Venaille, Y. Onuki, N. Perez, and A. Leclerc, From ray tracing to waves of topological origin in continuous media, *SciPost Physics* **14**, 062 (2023), [arXiv:2207.01479](https://arxiv.org/abs/2207.01479) [physics.flu-dyn].
- [64] P. Delplace, T. Yoshida, and Y. Hatsugai, Symmetry-Protected Multifold Exceptional Points and Their Topological Characterization, *Physical Review Letters* **127**, 186602 (2021).